AD-A035 508 ROME AIR DEVELOPMENT CENTER GRIFFISS AFB N Y F/G 17/9
COMPARISON OF MODELS FOR CALCULATING THE EFFECT OF RADOME DAMAG--ETC(U)
OCT 76 R J PAPA, R L TAYLOR

UNCLASSIFIED RADC-TR-76-320 NL

1 OF 1
AD-A
035 508

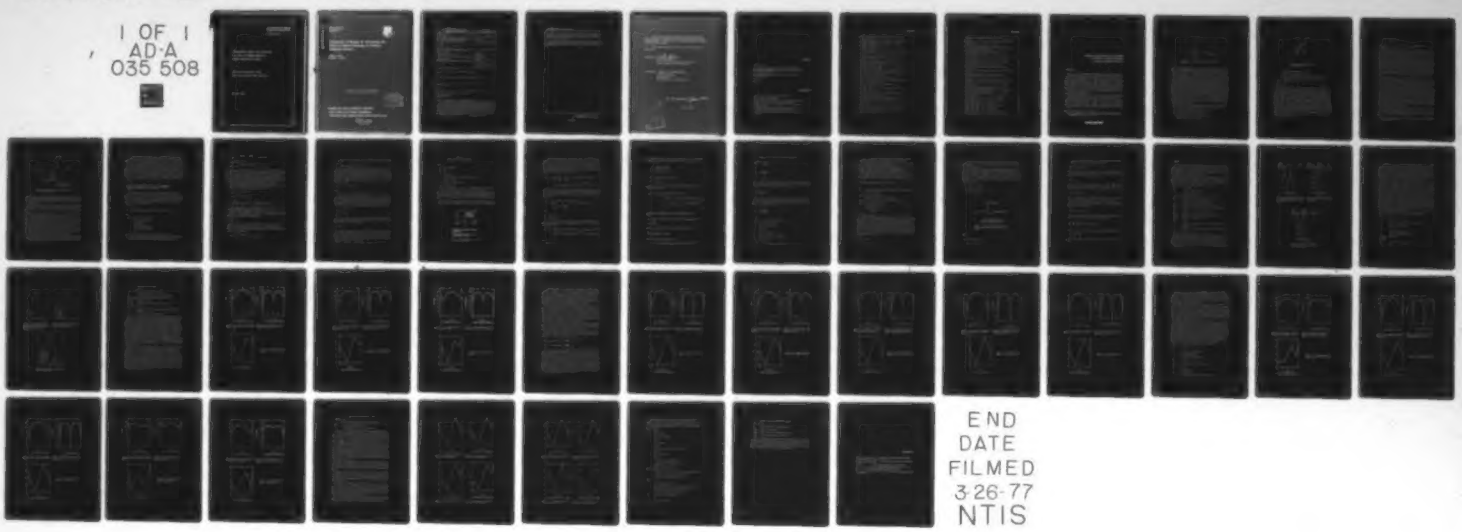

END
DATE
FILMED
3-26-77
NTIS

COMPARISON OF MODELS FOR CALCULATING THE EFFECT OF RADOME DAMAGE ON ANTENNA RADIATION PATTERNS

ROME AIR DEVELOPMENT CENTER
GRIFFISS AIR FORCE BASE, NEW YORK

OCTOBER 1976

RADC-TR-76-320
IN-HOUSE REPORT
OCTOBER 1976

Comparison of Models for Calculating the Effect of Radome Damage on Antenna Radiation Patterns

ROBERT J. PAPA
RICHARD L. TAYLOR

ROME AIR DEVELOPMENT CENTER
AIR FORCE SYSTEMS COMMAND
GRIFFISS AIR FORCE BASE, NEW YORK 13441

Unclassified

SECURITY CLASSIFICATION OF THIS PAGE (When Data Entered)

REPORT DOCUMENTATION PAGE		READ INSTRUCTIONS BEFORE COMPLETING FORM
1. REPORT NUMBER RADC-TR-76-320	2. GOVT ACCESSION NO.	3. RECIPIENT'S CATALOG NUMBER
4. TITLE (and Subtitle) COMPARISON OF MODELS FOR CALCULATING THE EFFECT OF RADOME DAMAGE ON ANTENNA RADIATION PATTERNS		5. TYPE OF REPORT & PERIOD COVERED In-House 6. PERFORMING ORG. REPORT NUMBER
7. AUTHOR(s) Robert J. Papa Richard L. Taylor		8. CONTRACT OR GRANT NUMBER(s)
9. PERFORMING ORGANIZATION NAME AND ADDRESS Deputy for Electronic Technology (RADC/ETEP) Hanscom AFB Massachusetts 01731		10. PROGRAM ELEMENT, PROJECT, TASK AREA & WORK UNIT NUMBERS 61102F 21530302
11. CONTROLLING OFFICE NAME AND ADDRESS Deputy for Electronic Technology (RADC/ETEP) Hanscom AFB Massachusetts 01731		12. REPORT DATE October 1976 13. NUMBER OF PAGES 59
14. MONITORING AGENCY NAME & ADDRESS(if different from Controlling Office)		15. SECURITY CLASS. (of this report) Unclassified 15a. DECLASSIFICATION/DOWNGRADING SCHEDULE

16. DISTRIBUTION STATEMENT (of this Report)

Approved for public release; distribution unlimited.

17. DISTRIBUTION STATEMENT (of the abstract entered in Block 20, if different from Report)

18. SUPPLEMENTARY NOTES

19. KEY WORDS (Continue on reverse side if necessary and identify by block number)

Monopulse radar system
Radome damage
Boresight error

20. ABSTRACT (Continue on reverse side if necessary and identify by block number)

Several different computer models have been developed for calculating the far-field radiation patterns of monopulse radar antennas covered by a damaged radome. The damaged portion of the radome (patch area) is characterized by a complex dielectric constant which differs from the unperturbed radome material. The computer models are used to study boresight shifts in the monopulse difference patterns for various patch shapes, patch sizes, and patch locations. The effect of the patch shape and location on the tracking signal is also

DD FORM 1 JAN 73 1473 EDITION OF 1 NOV 65 IS OBSOLETE

Unclassified

SECURITY CLASSIFICATION OF THIS PAGE (When Data Entered)

20. (Cont.)

investigation of null width effects on sidelobe levels, the experimental study of an element and control circuitry for two-dimensional scan, bandwidth effects, and the use of dielectric spatial filters and row displacement for residual grating lobe suppression.

In addition to these new results, data are given to enable the designer to determine element size and the minimum number of elements for arrays with approximately -20 dB grating lobes, and with near sidelobes reduced far below these levels.

This report has been reviewed by the RADC Information Office (OI) and is releasable to the National Technical Information Service (NTIS). At NTIS it will be releasable to the general public, including foreign nations.

This technical report has been reviewed and approved for publication.

APPROVED: Walter Rotman

WALTER ROTMAN
Chief, Microwave Detection Techniques Br.
Electromagnetic Sciences Division

APPROVED: Allan C. Schell

ALLAN C. SCHELL
Acting Chief
Electromagnetic Sciences Division

FOR THE COMMANDER: John P. Huss

Plans Office

Contents

Illustrations

Comparison of Models for Calculating the Effect of Radome Damage on Antenna Radiation Patterns

1. INTRODUCTION

In a previous report[1] three different mathematical models were developed to describe the shift in boresight axis of a monopulse antenna covered by a damaged radome. The dielectric properties of a radome may be altered as the result of structural changes induced by damage. In the present report two additional mathematical models are given to describe the shift in boresight axis of a monopulse antenna covered by a damaged radome. Graphs are presented of the sum and difference patterns for various sizes, shapes, and locations of the damaged portion (patch area) of the radome. Comparisons are made between the various models. Also, the effect on the boresight axis of a noise source in the near field of the monopulse antenna is investigated.

As explained in Papa and Taylor,[1] the first model (hereafter denoted MI) takes into account the effects of the damaged portion of the radome (patch area) by a simple aperture blocking model (see Figure 1). The patch is in the near field of the antenna. As a first approximation, diffraction of the rays around the edges of the patch will be neglected. As seen in Figure 1, the method of analysis consists in projecting the patch area directly back into the aperture plane. The aperture is

(Received for publication 12 October 1976)

1. Papa, R.J. and Taylor, R.L. (1975) Effect of Radome Damage on Antenna Tracking Systems, AFCRL-TR-75-0541.

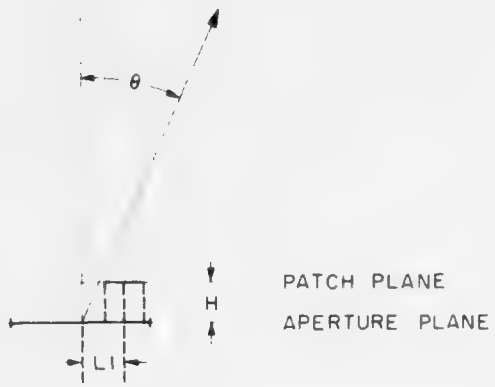

Figure 1. Simple Aperture Blocking Model Square Aperture

assumed to be rectangular for MI. For the monopulse system considered in this report, the amplitude distribution is taken to be uniform over the aperture plane and the phase distribution is varied to give two simultaneous beams. The patch may have various shapes: triangular, rectangular, circular, or elliptical.

The total aperture plane is divided into two parts: (1) the portion corresponding to the unperturbed aperture (UA) and (2) the portion corresponding to the projected patch area (PPA). The amplitude distribution in the PPA equals the amplitude distribution that originally existed in the unperturbed aperture times the amplitude of the complex transmission coefficient of the patch. The phase distribution in the PPA equals the phase distribution that originally existed in the unperturbed aperture plus the phase of the complex transmission coefficient of the patch plus $(2\pi/\lambda_o)D_p$ where λ_o = free-space wavelength and D_p = difference in optical path length from point on patch to point on aperture directly below the patch. The total aperture plane (TA) is given by TA = UA + PPA. The far-field pattern of two simultaneous lobes and the difference pattern of two simultaneous lobes are calculated for various patch shapes, patch locations, and patch sizes by taking the Fourier transform of the TA.

The second model (hereafter denoted by MII) is illustrated in Figure 2. In MII, the antenna is free to rotate with a gimbal angle = θ_A. In Figure 2,

θ_P = patch inclination angle with respect to vertical,

θ_T = angle of target with respect to vertical,

H = height of patch center above center of aperture,

z = distance above center of aperture,

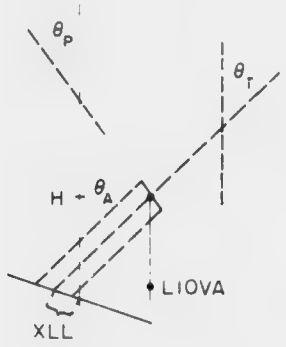

Figure 2. Modified Aperture Blocking Model

A = aperture width (parallel to x - axis),

B = aperture height (parallel to y - axis),

L1 = x displacement of center of patch from center of aperture,

L2 = y displacement of center of patch from center of aperture,

L1OVA = L1/A,

L2OVB = L2/B.

As illustrated in Figure 2, when the monopulse antenna is operating in the receiving mode, a plane wave emanating from the target will cast a shadow of the patch onto the aperture plane. In MII, a plane wave emanating from the target will cast a shadow of the patch onto the aperture plane. Also, the shadow of the patch will move as the target position changes. As in MI, the aperture plane in MII is divided into two parts: the unperturbed aperture (UA), and the projected patch area (PPA), where now the PPA has a different shape, in general, than the original patch. The far-field pattern is obtained by taking the Fourier transform of the total aperture plane (TA). The sum and difference patterns of a monopulse antenna are calculated for different patch sizes and locations. Also, the tracking signal TTT is calculated as a function of target angle, θ_T. If Σ represents the sum pattern (electric field intensity) and Δ represents the difference pattern, then the tracking signal is defined as

$$TTT = \frac{|\Sigma + \Delta| - |\Sigma - \Delta|}{|\Sigma + \Delta| + |\Sigma - \Delta|} \quad , \tag{1}$$

where | | denotes absolute value. The tracking signal vanishes when the target is on boresight.

The third mathematical model (MIII) to describe boresight shifts due to damaged radomes consists of a plane-wave spectrum – surface integration technique, discussed by Wu and Rudduck.[2] The plane-wave spectrum – surface integration method consists in making the following steps: (1) the near field of the antenna is calculated at a number of points on the inner surface of the radome, (2) the transmitted fields are calculated through the radome surface using ray-tracing techniques, (3) the far-field radiation pattern is calculated by numerically evaluating the Kirchhoff-Huygens integral expression for the fields outside of a closed surface in terms of the electric and magnetic current densities on the surface. In Reference 1 there is a discussion of the way the plane-wave spectrum – surface integration technique is used to calculate, for a monopulse antenna, the radiation pattern distortion produced by a damaged portion on the radome surface.

As indicated in Figure 3, the damaged portion (patch area) of the ogival radome corresponds to the intersection of a cylinder and an ogive. The complex dielectric coefficient K of the damaged portion of the radome is different from K for the unperturbed radome. The far-field radiation pattern for the sum pattern of a circular aperture is calculated for different patch sizes and locations.

In the fourth mathematical model (MIV) for calculating the boresight shift due to radome damage, the technique is essentially the same as in MII (see Figure 2), except that the complex transmission coefficient ($TR\, e^{i\phi TR}$) of the patch is not specified a priori. Instead, the complex dielectric coefficient K of the patch area is specified. Then, the computer program calculates the complex transmission coefficient corresponding to a plane wave emanating from the target and incident upon a dielectric slab with a predetermined thickness. Again, the sum pattern, difference pattern, and tracking signal of a monopulse system are calculated as a function of patch size, shape, and location.

In the fifth mathematical model (MV), the technique is the same as in MI (see Figure 1), except that the patch is coplanar with the aperture, so that $D_p = 0$. Also, the patch is taken to be rectangular, with sides parallel to the rectangular aperture. This permits one to obtain analytic expressions for the sum and

2. Wu, D.C.F. and Rudduck, R.C. (1974) IEEE Trans. on Antennas and Propagation, AP-22, No. 3:497.

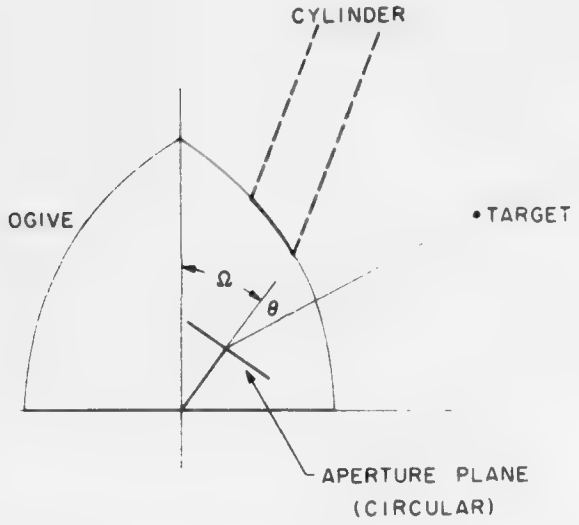

Figure 3. Ogival Radome, Plane-Wave Spectrum — Surface Integration Method

difference patterns of the monopulse antenna when a rectangular patch with a complex transmission coefficient is partially blocking the aperture. Again, the sum and difference patterns and the tracking signal are investigated as a function of the system parameters.

Graphs of the sum pattern, difference pattern, and tracking signal are plotted as a function of θ, where $\theta = \theta_T - \theta_A$, θ_T = angle of target, and θ_A = (gimbal) angle of antenna. In this report, MII is compared with MV and MIII is compared with MIV.

The effect on the boresight axis of a noise source in the near field is investigated. The noise emanates from the damaged portion of the radome. It is assumed that the dimensions of the noise source are much less than the distance of the source to any point in the antenna aperture plane. Thus, the noise source is considered to be a point source. If R_1 is the distance from the point noise source to one extremum of the aperture plane and R_2 is the distance from the noise source to another extremum of the aperture plane, then for a wave packet emitted from the source $\tau_D = (R_1 - R_2)/c$ is the time delay in receiving this wave packet at two observation points on the aperture plane. It is assumed that the correlation time τ_c of the noise source is long compared with τ_D.

Using MV, it is possible to obtain an analytic representation of the gain of the monopulse receiving antenna whose aperture is partially blocked by a rectangular patch with a complex transmission coefficient. Using this expression for the gain

of the monopulse receiving antenna in the radar range equation, it is possible to calculate the signal intensity at the detector of the antenna receiving system as a function of the system parameters (range, gain of transmitter, gain of receiver system, target cross section, power of transmitter, frequency of transmitter).

Under the assumptions that the noise source can be treated as a point source and $\tau_c \gg \tau_D$, it is possible to calculate the noise intensity at the detector of the antenna receiving system as a function of the system parameters (temperature of noise source, position of noise source with respect to aperture plane, dimensions of aperture, gain of receiver system, bandwidth of receiver system). Once the signal to noise ratio is determined at the detector of the antenna receiving system, it is possible to determine the angular uncertainty in boresight axis caused by the noise source.

2. COMPUTATIONAL METHODS FOR CALCULATING FAR-FIELD RADIATION PATTERNS OF MONOPULSE ANTENNAS COVERED BY A DAMAGED RADOME

The computational methods for MI, MII, MIII are discussed in Papa and Taylor.[1] In this report, as in Papa and Taylor,[1] the field variables E and H are assumed to vary in time as exp ($-i\omega t$). As explained in Reference 1, if the deviations from constant phase over the aperture are small, and if the field is uniformly polarized over the aperture, then the electric field intensity in the far field (Fraunhofer region) may be written as

$$E_F = \int d\eta \int d\xi \; F(\xi, \eta) \exp\left[-ik(\sin\theta \cos\phi \; \xi + \sin\theta \sin\phi \; \eta)\right] , \qquad (2)$$

where

$F(\xi,\eta)$ = aperture illumination factor,

θ = polar angle (see Figure 1),

ϕ = azimuthal angle,

ξ = abscissa in aperture plane,

η = ordinate in aperture plane,

k = ω/c.

In this report, only the principal plane will be considered ($\phi = 0^\circ$).

For a monopulse radar system with uniform amplitude aperture illumination, the unperturbed part of the aperture (UA) illumination factor is given by

$$F_{UA}^{S}(\xi, \eta) = e^{ik\sin\theta_o\xi} + e^{-ik\sin\theta_o\xi} = 2\cos(k \sin \theta_o \xi) \quad (3)$$

for the sum pattern, and

$$F_{UA}^{D}(\xi, \eta) = e^{ik\sin\theta_o\xi} - e^{-ik\sin\theta_o\xi} = 2i \sin(k \sin \theta_o \xi) \quad (4)$$

for the difference pattern. Here, θ_o is chosen so that the two main lobes of the monopulse system cross over at 3 dB down from the peak of each beam. In this report, the aperture is considered to be rectangular, of width A and height B. Let $F_{PPA}(\xi, \eta)$ represent the illumination factor in the projected patch area for MIV (see Figure 2); TR, the amplitude of the complex transmission coefficient of the patch area; ϕ_{TR}, the phase of the complex transmission coefficient of the patch area; and H, the height of the patch above the aperture plane.

For MIV, the amplitude of F_{PPA} equals the amplitude of F_{UA} times TR. The phase of F_{PPA} equals the phase of F_{UA} plus ϕ_{TR}, so that

$$F_{PPA} = F_{UA}\, TR\, e^{i\phi_{TR}} \quad . \quad (5)$$

Then, for $\phi = 0^o$, Eq. (2) becomes

$$E_F = \iint d\eta\, d\xi\, F_{UA}\, e^{-ik\sin\theta\xi} + \iint d\eta\, d\xi\, F_{PPA}\, e^{-ik\sin\theta\xi} \quad , \quad (6)$$

where F_{UA} is given by Eq. (3) for the sum pattern, F_{UA} is given by Eq. (4) for the difference pattern and F_{PPA} is given by Eq. (5).

In MIV, the shape and location of the PPA changes as the antenna look angle θ_A changes, or as the target angle θ_T changes. If θ is the angle of the target with respect to the unperturbed boresight axis, then

$$\theta = \theta_T - \theta_A \quad . \quad (7)$$

In Figure 2, XLL represents the distance from the center of the aperture to the center of the PPA. Also, L1OVA = L1/A where L1 = distance from center of patch to center of aperture along ξ-axis (abscissa), and A = aperture width. From Figure 2, it can be shown that

$$XLL = \cos\theta_T \cdot [L1OVA \cdot A - H \tan\theta_T] / \cos\theta \quad .$$

If

L2 = distance of center of patch to center of aperture along η-axis (ordinate)

and

B = aperture height, then L2OVB = L2/B.

Let RP represent the radius of a circular patch. To determine the geometrical shadow of the patch on the aperture plane due to a plane wave emanating from the target, consider a cylinder with the following properties: (1) the axis of the cylinder intersects the aperture plane at a poine ξ = XLL, η = L2; (2) the axis of the cylinder makes an angle θ_T with the vertical, and (3) the outer surface of the cylinder is tangent to the edge of the circular patch. The radius of this cylinder CYLR is given by

$$CYLR = RP \cdot \sin(\theta_T - \theta_P) \quad , \tag{8}$$

where

θ_P = angle of patch with respect to vertical.

The intersection of this cylinder with the aperture plane represents the geometrical shadow of the patch on the aperture plane. It is possible to determine whether a point on the aperture plane ξ, η lies within the shadow region. A point on the aperture plane ξ, η can be transformed into a coordinate system whose z-axis lies along the cylinder-axis by making the following transformations:

$$x_{CYL} = (\xi - XLL) \cos\theta \quad , \tag{9a}$$

$$y_{CYL} = (\eta - L2) \quad . \tag{9b}$$

Let $RR = x_{CYL}^2 + y_{CYL}^2$. Since the intersection of the cylinder with the aperture plane represents the shadow region, (generally an ellipse), a point on the aperture plane ξ, η lies within the shadow region if

$$RR \leq CYLR^2 \quad . \tag{10}$$

The complex transmission coefficient $TR\, e^{i\phi_{TR}}$ of the patch area is given by the transmission coefficient of a dielectric slab. The plane wave emanating from the target is incident on the dielectric layer. If it is assumed that the electric vector is perpendicular to the plane of incidence (transverse electric mode) then the transmission coefficient is given by:[3]

3. Born, N. and Wolf, E. (1965) Principles of Optics, Pergamon Press.

$$TR\, e^{i\phi_{TR}} = \frac{2q_1 q_2}{2q_1 q_2 \cos\beta - i \sin\beta\,(q_1^2 + q_2^2)} , \tag{11}$$

where

θ_i = angle of incidence ,

$q_1 = \cos\theta_i$,

$q_2 = \sqrt{K}\cos\theta_T$,

K = complex dielectric constant of slab (patch area) ,

$\beta = (2\pi/\lambda)\sqrt{K}\, h \cos\theta_T$,

h = thickness of dielectric slab ,

$\theta_T = \sin^{-1}[\sin\theta_i/\sqrt{K}]$.

The electric field in the far field may be calculated for MIV by combining Eqs. (3), (4), (5), (6), (7), (8), (9), (10), and (11). The sum pattern $(E_F \cdot E_F^*)_{SUM}$, the difference pattern $(E_F \cdot E_F^*)_{DIFF}$, and the tracking signal TTT given by Eq. (1) are calculated as a function of θ for different patch sizes, locations, antenna look angles θ_A, and complex transmission coefficients of the patch.

In MV, the patch is rectangular and coplanar with the rectangular aperture. When the sides of the rectangular patch are parallel to the aperture (see Figure 4),

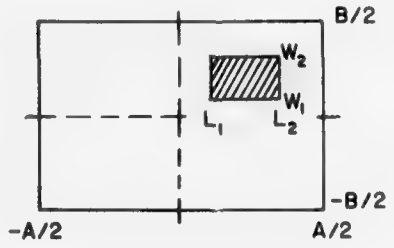

MONOPULSE APERTURE OF LENGTH A AND WIDTH B.

PATCH AREA OF LENGTH $L = L_2 - L_1$, AND WIDTH $W = W_2 - W_1$

Figure 4. Monopulse Aperture Covered by Partially Opaque Patch

then simple analytical expressions may be derived for the sum and difference patterns of the monopulse antenna. Let $U_y(w_1, w_2)$ be a unit step function which equals 1 when $w_1 \le y \le w_2$, and is zero elsewhere. Also, let $U_x(L_1, L_2)$ be a unit step function which equals 1 when $L_1 \le x \le L_2$ and is zero elsewhere. If PA represents the far field of the rectangular patch area and UA represents the far field of the unperturbed aperture, then Eqs. (2), (3), and (4) may be combined to yield the following expression for PA + UA:

$$PA + UA = \left(\frac{1}{AB}\right) \int_{-B/2}^{B/2} dy \int_{-A/2}^{A/2} dx \; e^{-ikx(S\theta - S\theta_o)} \pm e^{-ikx(S\theta + S\theta_o)} \cdot \left[1 + U_y(w_1, w_2)U_x(L_1, L_2) \cdot \left\{-1 + TR\, e^{i\phi_{TR}}\right\}\right] \tag{12}$$

where the far-field intensity has been normalized by dividing by the aperture area = AB. In Eq. (12), the plus sign is associated with the sum pattern and the minus sign is associated with the difference pattern. Also, the aperture illumination factor is given by

$$F(x, y) = \left(\frac{1}{AB}\right)\left[e^{-ikxS_-} \pm e^{-ikxS_+}\right] \cdot \left[1 + U_y(w_1, w_2)U_x(L_1, L_2) \cdot \left\{-1 + TR\, e^{i\phi_{TR}}\right\}\right], \tag{13}$$

where

$S_- = \sin\theta - \sin\theta_o$,

$S_+ = \sin\theta + \sin\theta_o$.

If $L = L_2 - L_1$, $w = w_2 - w_1$, and $L_A = ((L_1 + L_2)/2)$, then performing the integration in Eq. (12) yields the following expression for the far-field electric field intensity for MV:

$$PA + UA = SINXOVX(kAS_-/2) \pm SINXOVX(kAS_+/2) + (LW/AB)\left[-1 + TR\, e^{i\phi_{TR}}\right] \cdot \left[e^{-ikL_AS_-} SINXOVX(kLS_-/2) \pm e^{-ikL_AS_+} SINXOVX(kLS_+/2)\right] \tag{14}$$

where

$SINXOVX(x) = \sin x/x$.

Neglecting the obliquity factor cos θ in the expression (1 + cos θ), which multiplies the integral expression for the far-field pattern, the gain G may be written:[4]

$$G = \left(\frac{4\pi}{\lambda^2}\right) \frac{\left| \iint F(\xi, \eta)\, d\eta\, d\xi \right|^2}{\iint \left| F(\xi, \eta) \right|^2 d\eta\, d\xi} \quad , \tag{15}$$

where F is given by Eq. (13) for MV. Since

$$PA + UA = \iint F(\xi, \eta)\, d\eta\, d\xi$$

the numerator in Eq. (15) is given by the square of the right-hand side of Eq. (14). The denominator is given by

$$\begin{aligned} \iint \left| F(\xi, \eta) \right|^2 d\xi\, d\eta = \left(\frac{2}{AB}\right) \Big[& (1 - \text{SINXOVX}(kA \sin \theta_o)) \\ & + (LW/AB) \left\{ 1 - \cos (2kL_A \sin \theta_o)\, \text{SINXOVX}\, (kL \sin \theta_o) \right\} \\ & \cdot \left\{ 2(-1 + TR \cos \phi) + (1 - 2\, TR \cos \phi + TR^2) \right\} \Big] \quad . \end{aligned} \tag{16}$$

3. THE EFFECT ON THE BORESIGHT AXIS OF A NOISE SOURCE IN THE NEAR FIELD

For a signal with amplitude A, the rms error in measuring amplitude is

$$\delta A = (\overline{n^2})^{1/2} \quad ,$$

where n(t) is the amplitude of the noise. Thus, the relative error is

$$\frac{\delta A}{A} = \frac{1}{(A^2/\overline{n^2})^{1/2}} = \frac{1}{(2S/N)^{1/2}} \quad ,$$

where S/N is the signal to noise power ratio.

4. Silver, S. (1949) Microwave Antenna Theory and Design, McGraw Hill.

If TTT represents the tracking signal defined in Eq. (1), then

$$\frac{\delta(TTT)}{TTT} = \frac{1}{(2S/N)^{1/2}} \quad .$$

But,

$$\delta(TTT) = \frac{d(TTT)}{d\theta}\,\delta\theta \quad ,$$

$$= K_S\,\delta\theta \quad ,$$

where $K_s = \frac{d(TTT)}{d\theta}$ is the tracking sensitivity. Also, TTT is maximum at θ_B, the antenna beamwidth (one beam in the monopulse system). Thus, $\delta\theta$, the uncertainty in boresight axis due to the presence of noise, is given by:[5]

$$\delta\theta = \frac{\theta_B}{K_S\sqrt{2S/N}} \quad . \tag{17}$$

The noise emanates from the damaged portion of the radome (patch area), which lies in the near field of the antenna. The signal power received by the monopulse antenna partially covered by an opaque patch (Figure 4) is given by the radar range equation (cw system)

$$P_R = \frac{P_t G_t G_r \lambda^2 \sigma_T}{(4\pi)^3 R_1^2 R_2^2} \quad , \tag{18}$$

where

P_R = power received by monopulse antenna,

G_t = gain of transmitting antenna,

G_r = gain of receiving antenna,

λ = wavelength,

σ_T = target cross section,

R_1 = range from transmitter to target,

R_2 = range from target to receiving antenna,

P_t = transmitted power.

5. Barton, D.K. (1964) Radar Systems Analysis, Prentice Hall, p. 282.

In Eq. (18) the gain G_r of the receiving monopulse antenna with partially blocked aperture is obtained by combining Eqs. (14), (15), and (16).

In Eq. (17) for the uncertainty in boresight axis $\delta\theta$ due to noise, the parameters on the right-hand side are determined as follows:

(1) The antenna beamwidth θ_B may be calculated from Eq. (14) and Eq. (1), as that angle at which the tracking signal TTT reaches a maximum.

(2) The tracking sensitivity K_s is equal to $\frac{d(PA + UA)}{d\theta}$ in Eq. (14).

(3) The signal power level S at the detector is given by $G_{REC} \cdot P_r$ where G_{REC} is the gain of the receiver system and P_r is given by Eq. (18).

(4) The noise power level N at the detector is calculated from the relation

$$N = P_N^R G_{REC} + kT_{SKY}^A B G_{REC} G_r + kT_{REC} B G_{REC} \quad , \tag{19}$$

where

P_N^R = noise power at receiving antenna aperture due to external noise source in near field,

G_{REC} = gain of receiver system,

B = bandwidth of antenna plus receiver system,

T_{REC} = noise temperature of receiver system (effective),

T_{SKY}^A = average sky temperature,

$$= \frac{\int T_{SKY}(\theta, \phi)\, G_r(\theta, \phi)\, d\Omega}{\int G_r(\theta, \phi)\, d\Omega}$$

and G_r is given by Eq. (15).

As indicated in the introduction, P_N^R (the noise power captured at the antenna aperture due to an external noise source in the near field) is calculated by making two fundamental assumptions: (a) The noise emanates from the damaged portion of the radome. It is assumed that the dimensions of the noise source are much less than the distance of the source to any point in the aperture plane. Then, the noise source may be considered a point source. (b) If R_1 is the distance from the point noise source to one extremum of the aperture plane and R_2 is the distance from the noise source to another extremum in the aperture plane, then for a wave packet emitted from the source

$$\tau_D = (R_1 - R_2)/c$$

is the time delay in receiving this wave packet at two observation points on the aperture plane. It is assumed that the correlation time τ_c of the noise source is long compared to τ_D.

Under assumptions (a) and (b), it is possible to calculate the noise power captured at the aperture plane P_N^R by first subdividing the aperture plane into subsections of length $\ell_x = A/N$ and width $\ell_y = B/M$, where both ℓ_x and ℓ_y are less than or equal to one half wavelength. From Figure 5 it may be seen that L_1, L_2, H represent the x, y, z coordinates of the noise source. Then, $x_1 = A/2 - L_1 - \ell_x/2$ represents the distance from the center of the first subsection to the noise source along the x-axis, and

$$x_2 = A/2 - L_1 - 3\ell_x/2 ,$$

$$x_3 = A/2 - L_1 - 5\ell_x/2 ,$$

$$x_N = A/2 - L_1 - (2N - 1)\,\ell_x/2 ,$$

$$= -A/2 - L_1 + \ell_x/2 .$$

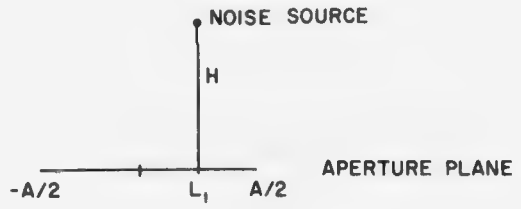

$\ell_x = A/N$ = LENGTH OF SMALL SUBSECTION OF APERTURE PLANE

Figure 5. Position of Noise Source in Near Field of Antenna with Respect to Aperture Plane

Similarly,

$$y_1 = B/2 - L_2 - \ell_y/2 ,$$

$$y_N = -B/2 - L_2 + \ell_y/2 .$$

If x_i is the x-coordinate of the center of a particular subsection of the aperture plane and y_j is the corresponding y-coordinate, then

$$R_{ij} = \left[H^2 + x_i^2 + y_j^2\right]^{1/2}$$

is the distance from the noise source to the center of this subsection. Also, if T_N is the temperature of the noise source, B is the bandwidth of the entire receiving system, and k = Boltzmann's constant, then

$$P_T^E = kT_N B \tag{20}$$

is the total noise power emitted by the noise source, and $E_T^E = \sqrt{P_T^E}$ is proportional to the rms electric field amplitude of the emitted noise power. Then, assuming that the noise source is an isotropic radiator and is randomly polarized,

$$E_{ij} = E_T^E(\ell_x \ell_y)/(4\pi R_{ij}^2) \quad , \tag{21}$$

where E_{ij} is proportional to the amplitude of the rms electric field intensity of the noise captured by the ijth subsection of the aperture plane (x_i, y_j).

If the phase distribution across the aperture of the monopulse antenna is adjusted to give the difference pattern, then the phase factor associated with the amplitude E_{ij} in Eq. (21) is given by

$$e^{-ikR_{ij}} \sin [kx_i \sin \theta_o] \quad . \tag{22}$$

If E_N^R is proportional to the total electric field amplitude at the antenna aperture due to an external noise source in the near field, then

$$E_N^R = \sum_{i=1}^{N} \sum_{j=1}^{M} E_{ij}\, e^{-ikR_{ij}} \sin [kx_i \sin \theta_o] \quad . \tag{23}$$

The total noise power received over the entire antenna aperture is given by

$$P_N^R = (E_N^R) \cdot (E_N^R)^* \quad . \tag{24}$$

This may be substituted into Eq. (19) to obtain the total noise power N at the detector.

4. CONCLUSIONS

For MI, MII, and MIV, the rectangular aperture integrations were performed using Simpson's rule with Richardson's extrapolations.[6] In MIII, the plane wave spectrum integrations for the near fields of a circular aperture were performed using Simpson's rule (sum pattern), and the Kirchhoff integrals over the radome surface were evaluated using the trapezoidal rule.

In Figures 6, 7, and 8, the sum pattern of a circular aperture is indicated as a function of polar angle θ, calculated according to MIII. These figures correspond to Figures 63, 64, and 68 of Reference 1. The circular aperture is uniformly illuminated. The damaged portion of the radome corresponds to the intersection of a cylinder with an ogive. In Figures 6, 7, and 8,

RIB = $R1/\lambda = 14.0$,

R1 = radius of generator of ogive ,

λ = free space wavelength ,

CYLRADB = (Height of ogive from base to vertex)/λ = 12.124 ,

THETAC = Angle that cylinder axis makes with vertical ,

Ω = Gimbal angle of antenna (see Figure 3) ,

N^R_{RAD} = Real part of index of refraction of unperturbed radome ,

N^I_{RAD} = Imaginary part of index of refraction of unperturbed radome = 0.0 ,

N^R_{PAT} = Real part of index of refraction of patch area ,

N^I_{PAT} = Imaginary part of index of refraction of patch area ,

TRADB = (thickness of radome wall)/λ ,

XL3B = $L3/\lambda$,

L3 = Distance from base center of ogive to center of aperture (see Figure 3) ,

P_o = Power radiated into far field at angle θ normalized to power at $\theta = 0^o$.

HXSNUM = (Height of ogive from base to vertex)/λ.

In Figure 6, the complex dielectric constants of both unperturbed radome and patch area correspond to free space (K = 1.0). In Figure 7, the dielectric constant of the patch area is the same as the unperturbed part of the radome. The thickness of the radome wall is adjusted so that it equals $(1/2)\lambda_R$, where

6. McCormick, J.M. and Salvadori, M.G. (1964) Numerical Methods in Fortran, Prentice-Hall.

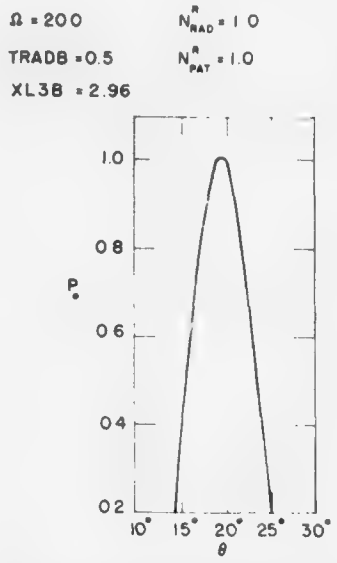

Figure 6. Sum Pattern of Circular Aperture (MIII), Far Field of Circular Aperture, Integration Over Small Ogival Surface

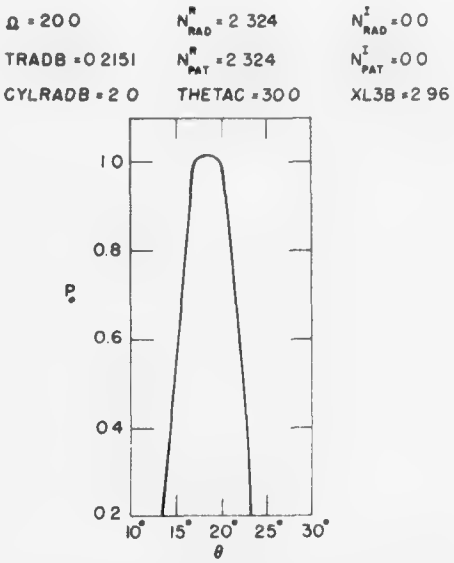

Figure 7. Sum Pattern of Circular Aperture (MIII), Effect of Radome, Small Ogive

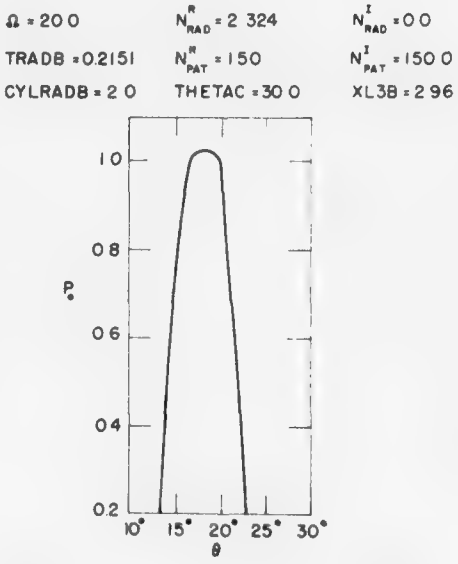

Figure 8. Sum Pattern of Circular Aperture (MIII), Effect of Conducting Patch, Small Ogive

λ_R = wavelength in radome material. This minimizes reflection loss. Comparing Figure 7 with Figure 6, it may be seen that the radome itself, with no effective damage area, introduces a boresight shift of about one degree. In Figure 8, the real and imaginary parts of the complex index of refraction are large for the patch area, corresponding to a conducting patch of about four wavelengths in diameter (the patch area is egg-shaped, as shown in Figure 44 of Reference 1). Comparing Figure 8 with Figure 7 shows that the conducting patch on the radome surface introduces no further boresight shift in the sum pattern.

In Figures 9, 10, and 11, the sum pattern of a circular aperture is also calculated according to MIII, but the dimensions of the ogive are much larger than the dimensions corresponding to Figures 6, 7, and 8. Now, RIB = 117.43 and HXSNUM = 36.83. Figures 9, 10, and 11 correspond to Figures 50, 51, and 55 of Reference 1: In Figure 9, the complex dielectric constants of both unperturbed radome and patch area correspond to free space (K = 1.0). In Figure 10, the complex dielectric constant of the patch area equals that of the unperturbed radome, so that there is effectively no radome damage. Comparing Figure 10 with Figure 9 shows that the presence of the radome, with wall thickness = $\lambda_R/2$ to minimize reflection, introduces no boresight shift. In Figure 11, the real and imaginary parts of the complex index of refraction are large for the patch area, again corresponding to an egg-shaped conducting patch on the ogival surface (see Figure 41 of Reference 1). Comparing Figure 11 with Figure 9 shows that the conducting patch introduces no boresight shift.

Figures 12 through 29 correspond to MIV, with a uniformly illuminated rectangular aperture and a circular patch area. In these figures,

KH	= $(2\pi/\lambda)H$,
K	= $2\pi/\lambda$,
H	= Height of center of patch above aperture plane
λ	= Free-space wavelength ,
L1OVA	= L1/A ,
L1	= Abscissa of center of patch ,
A	= Length of rectangular aperture ,
Radius of Circular Patch	= KA/SPSIZE ,
B	= Width of rectangular aperture ,
L2OVB	= L2/B ,

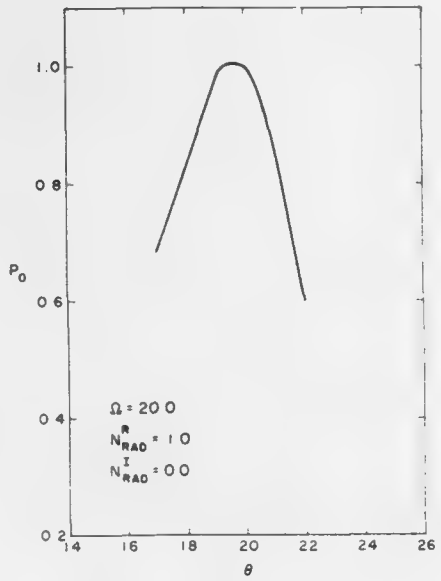

Figure 9. Sum Pattern of Circular Aperture (MIII), Far Field of Circular Aperture, Integration of Current Densities Over Radome Surface, Large Ogive

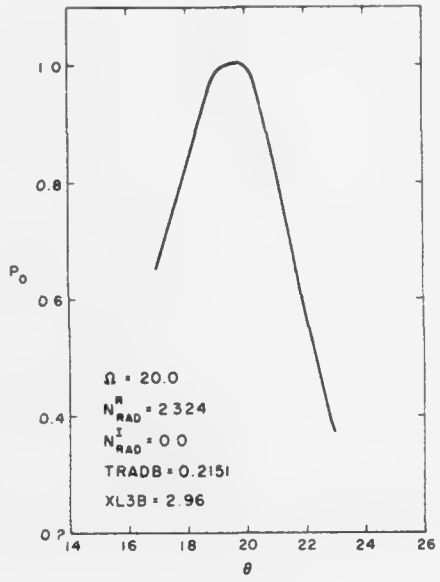

Figure 10. Sum Pattern of Circular Aperture (MIII), Effect of Radome (No Patch) Large Ogive

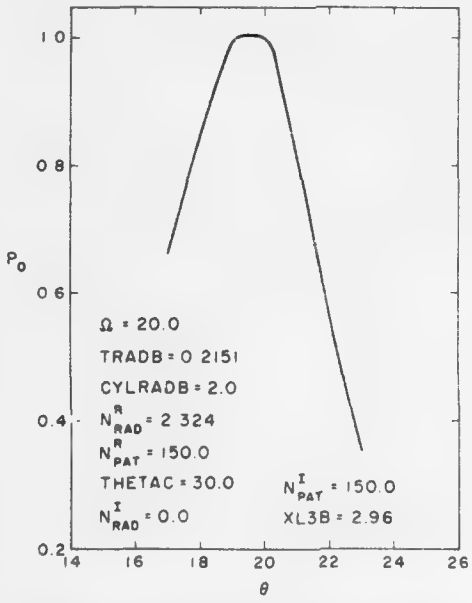

Figure 11. Sum Pattern of Circular Aperture (MIII), Effect of Conducting Patch (Large Ogive)

L2 = Ordinate of center of patch ,

θ = $\theta_T - \theta_A$,

θ_T = Angle of target with respect to vertical ,

θ_A = Gimbal angle of antenna with respect to vertical ,

THETAPA = Angle of plane of patch with respect to vertical ,

TPATB = (thickness of patch)/λ ,

ENPAT = Complex index of refraction of patch material ,

ETOTSSQ = $E_S \cdot E_S^*$,

E_S = Electric field intensity of difference pattern of monopulse antenna ,

TTT = Tracking signal, as defined in Eq. (1) .

In Figures 12 through 17, the size and position of the patch area are the same as in Figures 6, 7, and 8. The value of the complex index of refraction and the patch thickness corresponding to Figures 12, 13, and 14 are the same as in Figure 7. Allowing for the differences in scales, Figure 12 for the sum power pattern has approximately the same general shape as Figure 7. In Figures 15, 16, and 17, the real and imaginary parts of the complex index of refraction are large, so that the patch behaves as a conductor. The patch has the same characteristics (size, position, and complex index of refraction) in Figures 15, 16, and 17 as in Figure 8. Again, allowing for the differences in scales, Figure 15 for the sum pattern has the same general shape as Figure 8. Comparing Figure 13 with Figure 16 and Figure 14 with Figure 17, it may be noted that the difference patterns and tracking signals are approximately the same, regardless of whether the patch material is a dielectric or a conductor. This is true only for this particular patch size and position.

In Figures 18, 19, and 20, the patch radius is twice the radius corresponding to Figures 12 through 17 (four wavelengths instead of two wavelengths). In Figures 18, 19, and 20, the real and imaginary parts of the complex index of refraction are large, so that the patch behaves like a conductor. Comparing Figures 18, 19, and 20 with Figures 15, 16, and 17, it may be seen that an increase in the patch size has a pronounced effect on the monopulse radiation patterns. The large conducting patch tends to flatten and broaden the sum pattern, decrease the depth of the null in the difference pattern, and decrease the slope of the tracking signal (d(TTT)/dθ). The slope of the tracking signal, K_S = d(TTT)/dθ, is termed the tracking sensitivity. A decrease in tracking sensitivity decreases the tracking capabilities of the monopulse system.

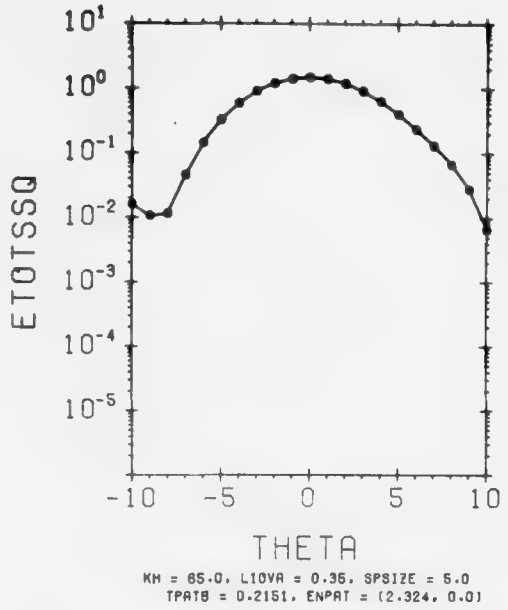

Figure 12. Sum Pattern of Rectangular Aperture (MIV), ENPAT = (2.324, 0.0) L1OVA = 0.35

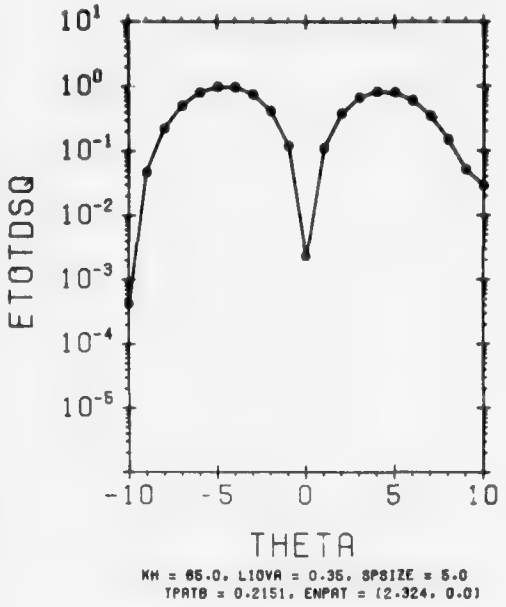

Figure 13. Difference Pattern of Rectangular Aperture (MIV), ENPAT = (2.324, 0.0), L1OVA = 0.35

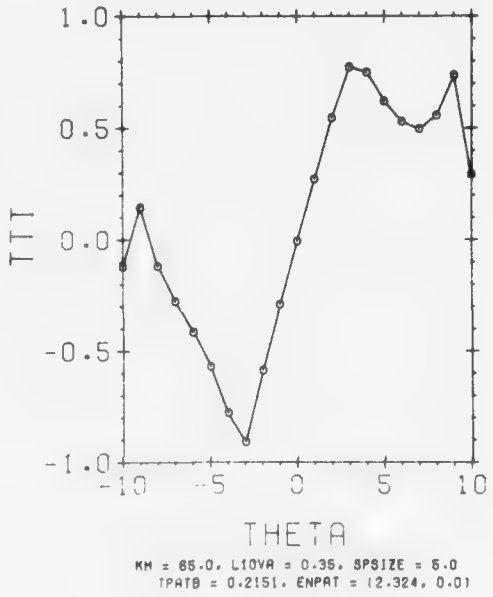

Figure 14. Tracking Signal (MIV), ENPAT = (2.324, 0.0), L1OVA = 0.35

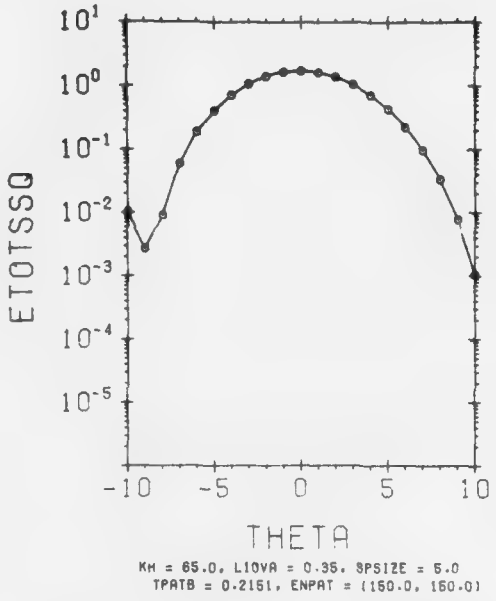

Figure 15. Sum Pattern of Rectangular Aperture (MIV), ENPAT = (150.0, 150.0) L1OVA = 0.35

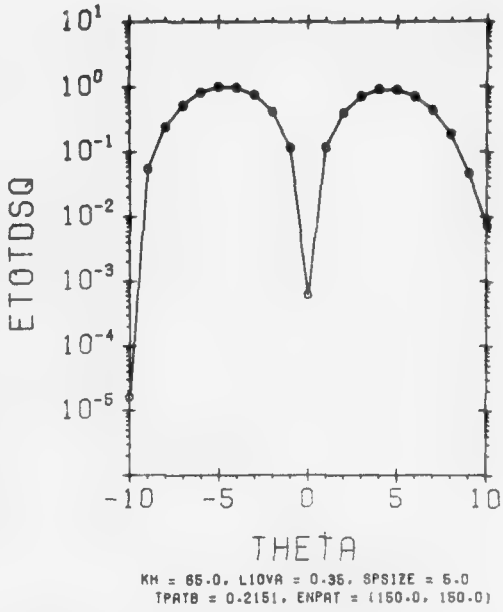

Figure 16. Difference Pattern of Rectangular aperture (MIV), ENPAT = (150.0, 150.0), L1OVA = 0.35

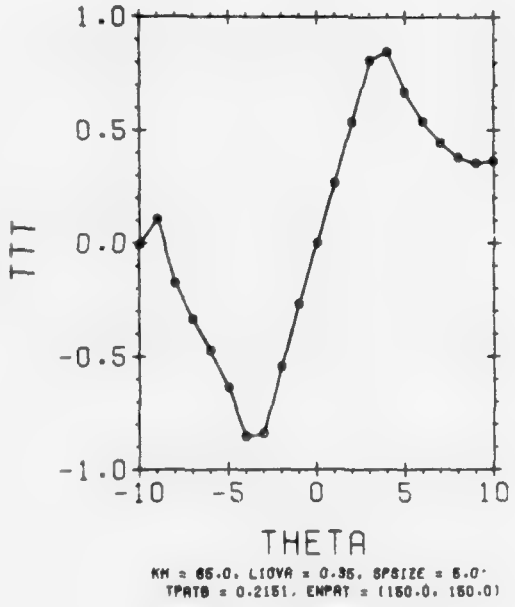

Figure 17. Tracking Signal (MIV), ENPAT = (150.0, 150.0) L1OVA = 0.35

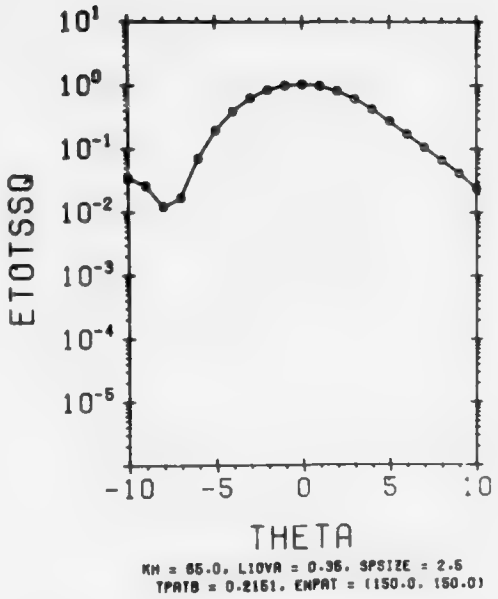

Figure 18. Sum Pattern of Rectangular Aperture (MIV), SPSIZE = 2.5

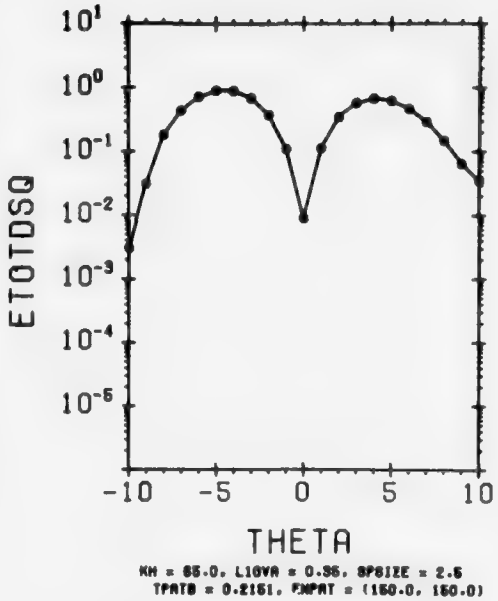

Figure 19. Difference Pattern of Rectangular Aperture (MIV), SPSIZE = 2.5

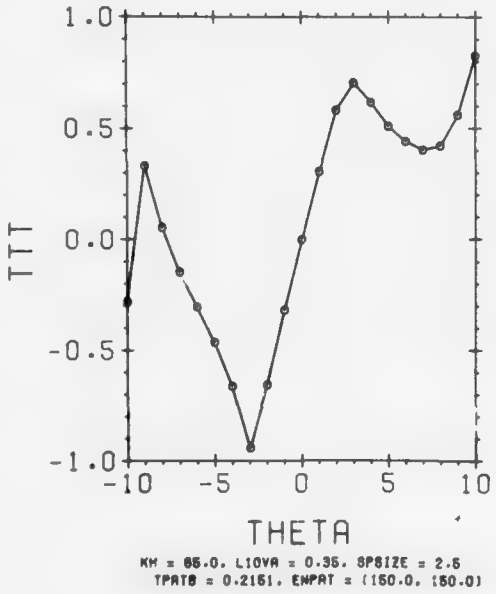

Figure 20. Tracking Signal (MIV), SPSIZE = 2.5

In Figures 21 through 29 (MIV), the size and location of the patch area are the same as in Figures 9, 10, and 11 (MIII). In Figures 21, 22, and 23, the patch thickness is zero (TPATB = 0.0), so that effectively there is no damaged portion of the radome. This corresponds to the parameters in Figure 9, calculated according to MIII. Allowing for scale changes, the general shape of the sum pattern in Figure 21 is the same as in Figure 9. From Figure 22, it may be observed how deep the null is in the difference pattern for the unperturbed radome. In Figure 23, the slope of the tracking signal K_S is at its maximum.

In Figures 24, 25, and 26, the dielectric constant of the patch area corresponds to that of the unperturbed radome, and the thickness of the patch is $\lambda_R/2$, where λ_R = wavelength in radome material. This corresponds to the value of the parameters in Figure 10. The sum pattern in Figure 24 (MIV) has the same general shape as the pattern in Figure 10 (MIII). Comparing Figure 25 with Figure 22 and Figure 26 with Figure 23, it may be seen that the dielectric patch produces a small amount of null filling in the difference pattern and a slight decrease in the tracking sensitivity. However, there is no boresight shift.

The real and imaginary parts of the complex index of refraction are large in Figures 27, 28, and 29, corresponding to a conducting patch. Since the parameters in Figure 27 are the same as in Figure 11, a comparison of the two figures shows the same behavior of the sum pattern as a function of θ.

Figures 30 through 50 correspond to MIV, with a uniformly illuminated rectangular aperture and a rectangular patch area. The parameters are defined in the same way as Figures 12 through 29, except that:

$$\text{length of rectangular patch} = \frac{KA}{SPSIZE} \quad ,$$

$$\text{width of rectangular patch} = \frac{KA}{SPSIZE} \quad .$$

In Figures 30, 31, and 32, the thickness of the patch is extremely small compared with a wavelength and the dielectric constant equals the free-space value. The antenna gimbal angle $\theta_A = 0^\circ$ in Figures 30 through 50. The tracking sensitivity K_S in Figure 32 is at its maximum. In Figures 33, 34, and 35, the center of the patch is located over the center of the aperture. The thickness of the patch = $\lambda_R/2$, where λ_r = wavelength in the material of the patch, so as to minimize reflections. The dielectric constant is equal to the value of the undamaged radome. Comparing Figures 33, 34, and 35 with Figures 30, 31, and 32, it may be noted that the patch whose dielectric constant equals the value of the unperturbed radome causes no boresight shift and no decrease in tracking sensitivity when the patch is symmetrically placed (centered) over the aperture.

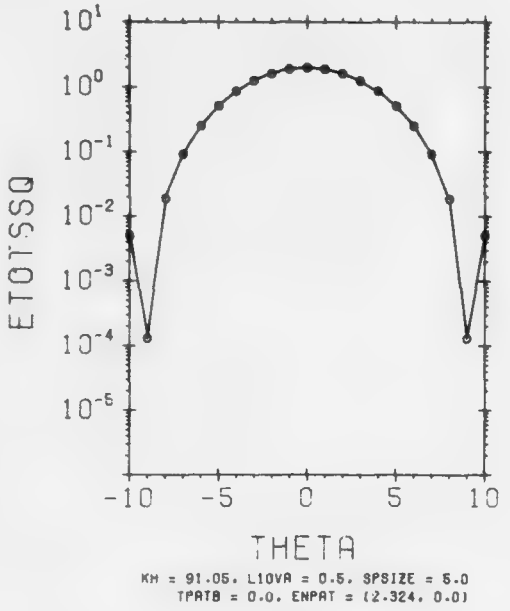

Figure 21. Sum Pattern of Rectangular Aperture (MIV), TPATB = 0.0

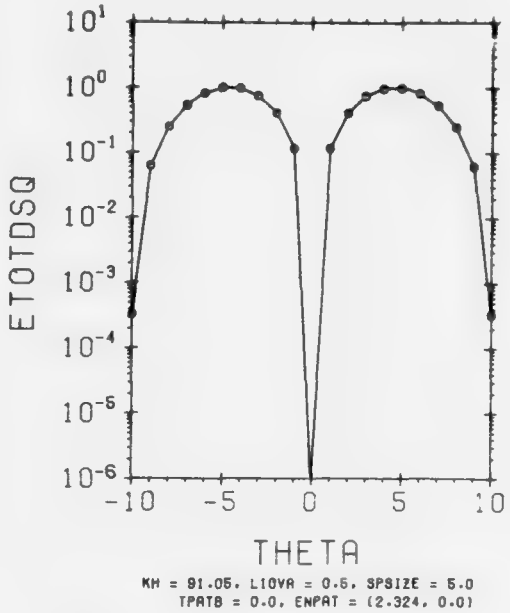

Figure 22. Difference Pattern of Rectangular Aperture (MIV), TPATB = 0.0

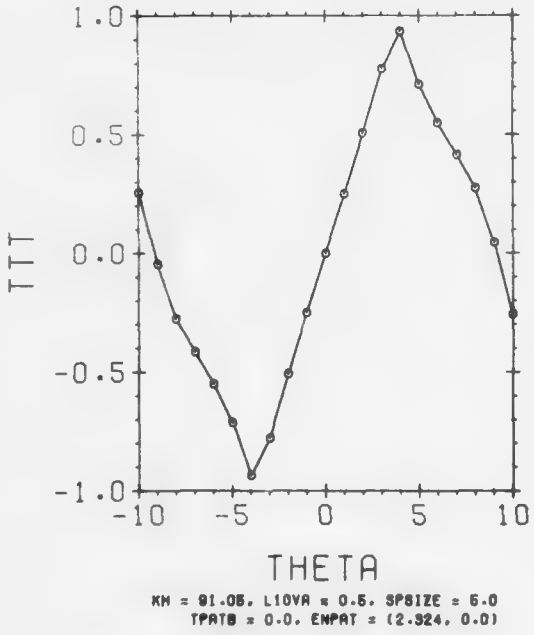

Figure 23. Tracking Signal (MIV), TPATB = 0.0

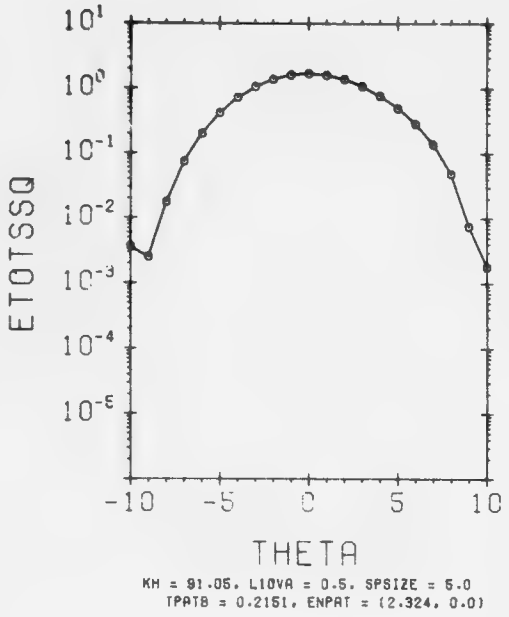

Figure 24. Sum Pattern of Rectangular Aperture (MIV), KH = 91.05, TPATB = 0.2151

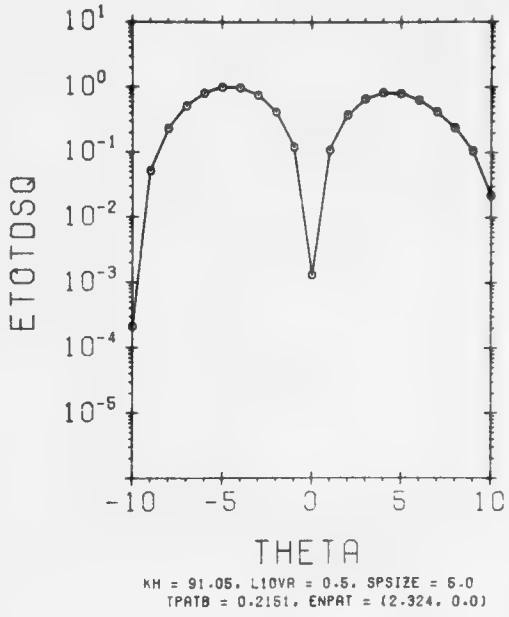

Figure 25. Difference Pattern of Rectangular Aperture (MIV), KH = 91.05, TPATB = 0.2151

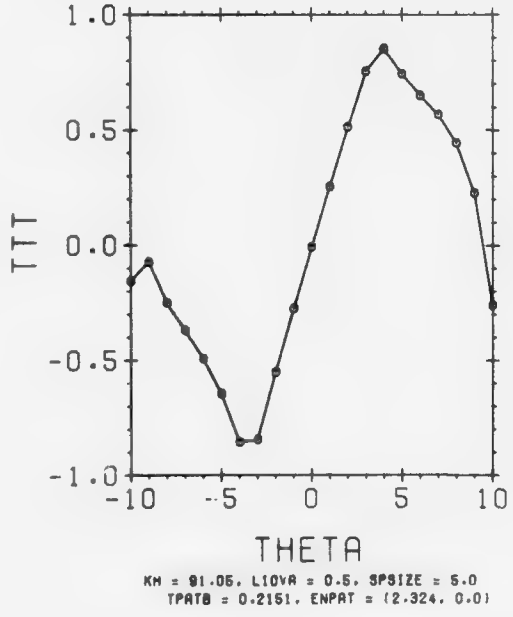

Figure 26. Tracking Signal (MIV), KH = 91.05, TPATB = 0.2151

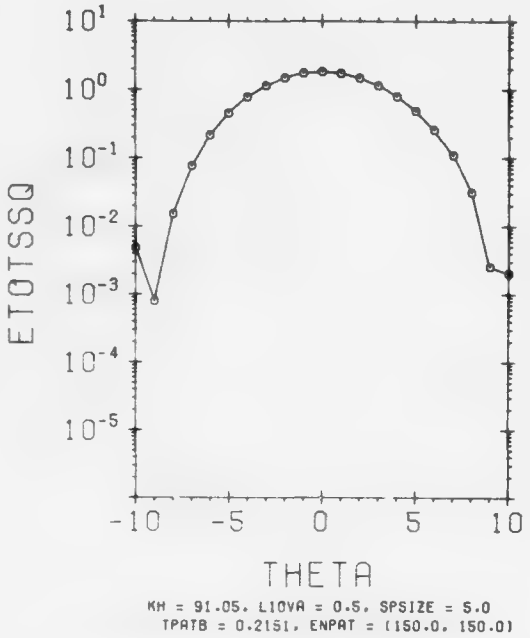

Figure 27. Sum Pattern of Rectangular Aperture (MIV), ENPAT = (150.0, 150.0), KH = 91.05, L1OVA = 0.5

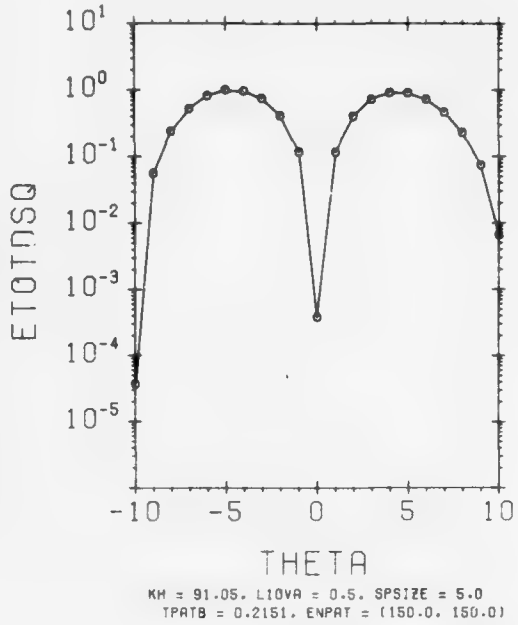

Figure 28. Difference Pattern of Rectangular Aperture (MIV), ENPAT = (150.0, 150.0), KH = 91.05, L1OVA = 0.5

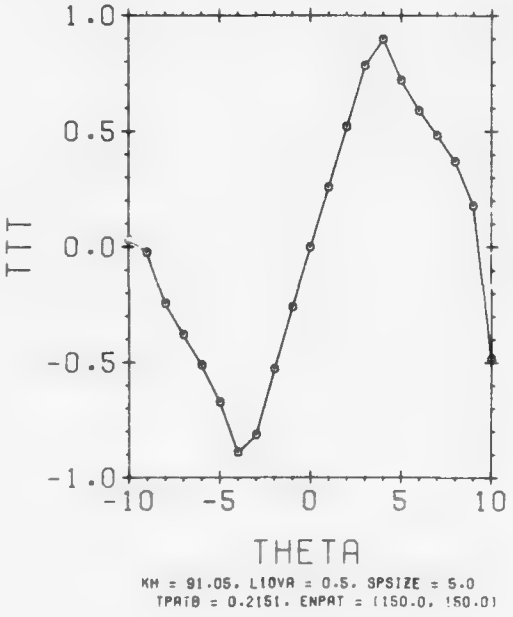

Figure 29. Tracking Signal (MIV), ENPAT = (150.0, 150.0), KH = 91.05, L1OVA = 0.5

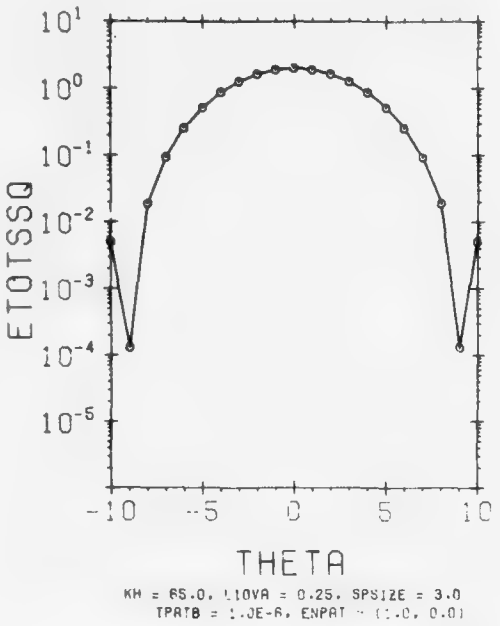

Figure 30. Sum Pattern of Rectangular Aperture (MIV), ENPAT = (1.0, 0.0), KH = 65.0

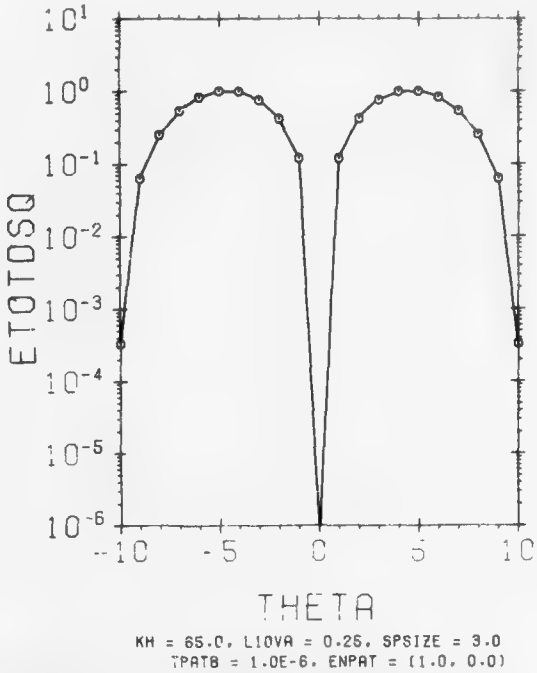

Figure 31. Difference Pattern of Rectangular Aperture (MIV), ENPAT = (1.0, 0.0), KH = 65.0

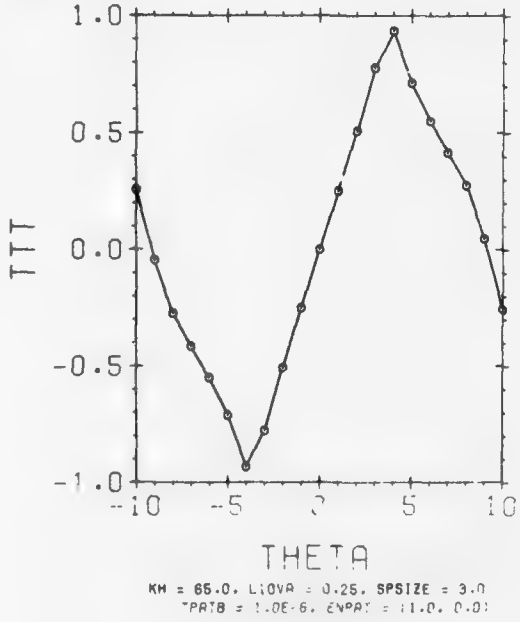

Figure 32. Tracking Signal (MIV), ENPAT = (1.0, 0.0), KH = 65.0

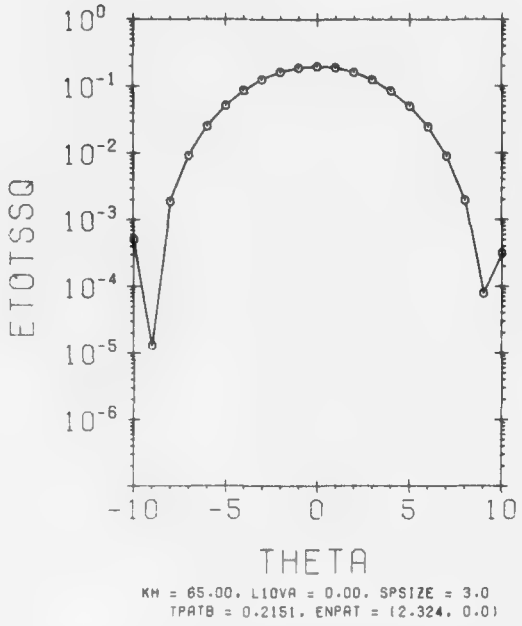

Figure 33. Sum Pattern of Rectangular Aperture (MIV), L1OVA = 0.00, KH = 65.0

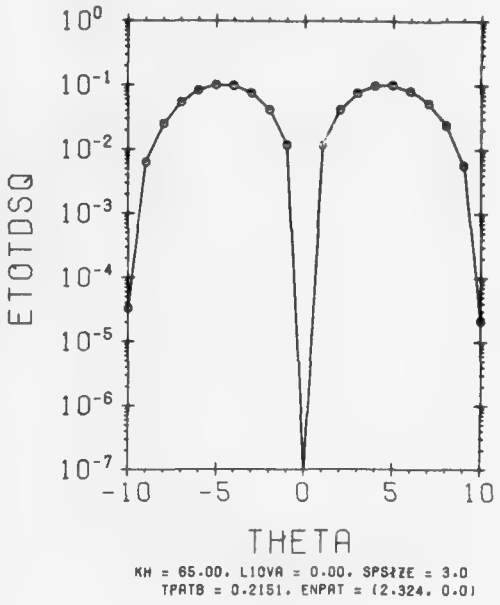

Figure 34. Difference Pattern of Rectangular Aperture (MIV), L1OVA = 0.00, KH = 65.0

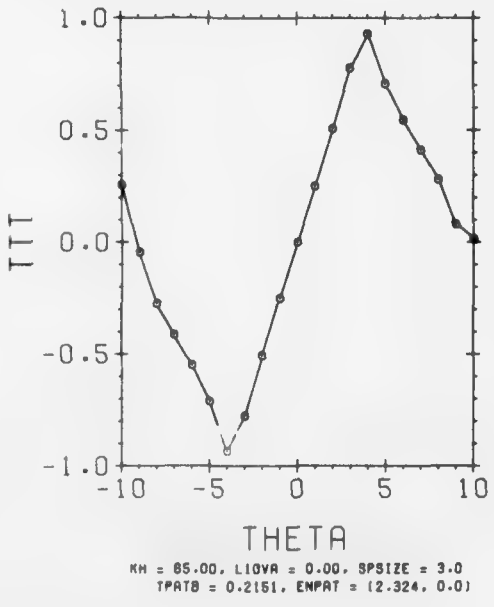

Figure 35. Tracking Signal (MIV), L1OVA = 0.00, KH = 65.0

In Figures 36, 37, and 38, the real and imaginary parts of the complex index of refraction of the patch are large (conducting patch), and the patch is not symmetrically centered over the aperture. Comparing Figures 36, 37, and 38 with Figures 30, 31, and 32, it may be seen that the asymmetrically located conducting patch produces null filling in the difference pattern and decreases the tracking sensitivity K_S, but there is no boresight shift.

The height of the patch center (KH) from the aperture plane in Figures 30 through 38 equals 65, whereas KH = 91.05 in Figures 39 through 50. In Figures 39, 40, and 41, the dielectric constant of the patch area is equal to the free space value. In Figures 42, 43, and 44, the dielectric constant of the patch area is equal to the value of the undamaged radome and the center of the patch is symmetrically located over the aperture. It may be seen that the symmetrically located dielectric patch produces no boresight shift and no decrease in K_S when Figures 42, 43, and 44 are compared with Figures 39, 40, and 41.

The parameters in Figures 45, 46, and 47 are the same as in Figures 42, 43, and 44, except that the center of the patch is asymmetrically located over the aperture plane (L1OVA = 0.25 instead of zero). It may be seen that the asymmetrically located dielectric patch virtually destroys the difference pattern, greatly distorts the tracking signal, and causes a boresight shift when Figures 45, 46, and 47 are compared with Figures 42, 43, and 44. The parameters in Figures 48, 49, and 50 correspond to a conducting patch asymmetrically located over the aperture. Comparing Figures 48, 49, and 50 with Figures 39, 40, and 41 shows that an asymmetrically located conducting patch causes considerable null filling in the difference pattern and decreases K_S, but there is no boresight shift.

Figures 51 through 58 correspond to MV. In these figures,

KA = $(2\pi/\lambda)A$,

K = $2\pi/\lambda$,

A = aperture length (rectangular) ,

λ = free space wavelength ,

L = patch length (rectangular patch) ,

KLA = $(2\pi/\lambda)LA$,

LA = position of center of patch along x-axis ,

WOVB = W/B ,

W = width of patch ,

B = aperture width ,

TR = magnitude of transmission coefficient of patch ,

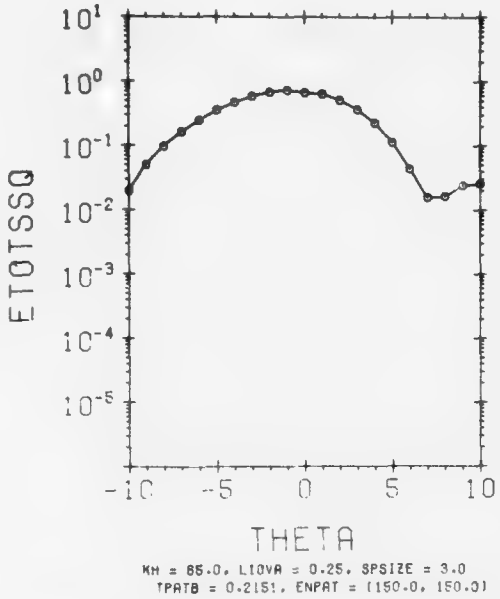

Figure 36. Sum Pattern of Rectangular Aperture (MIV), ENPAT = (150.0, 150.0), KH = 65.0, L1OVA = 0.25

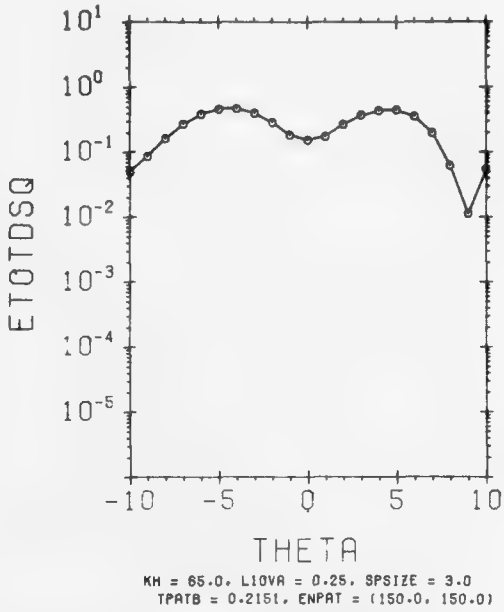

Figure 37. Difference Pattern of Rectangular Aperture (MIV), ENPAT = (150.0, 150.0), KH = 6.5, L1OVA = 0.25

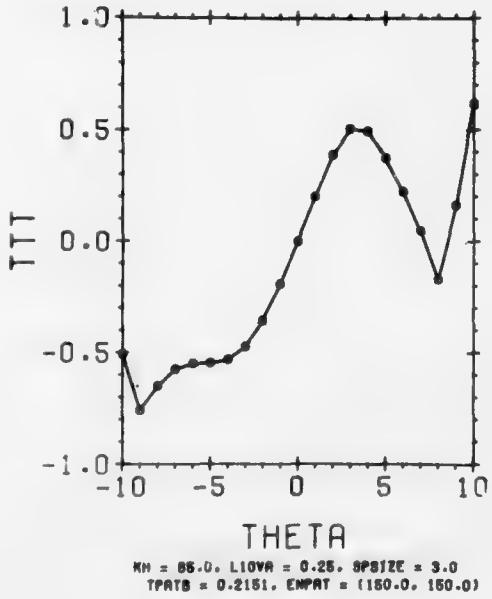

Figure 38. Tracking Signal (MIV), ENPAT = (150.0, 150.0), KH = 65.0, L1OVA = 0.25

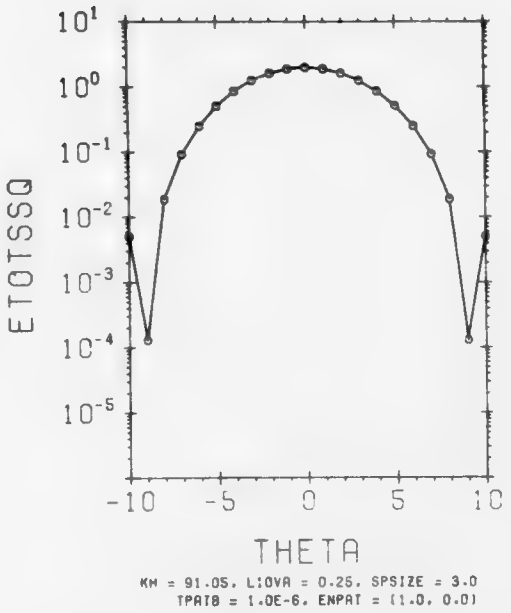

Figure 39. Sum Pattern of Rectangular Aperture (MIV), ENPAT = (1.0, 0.0), KH = 91.05

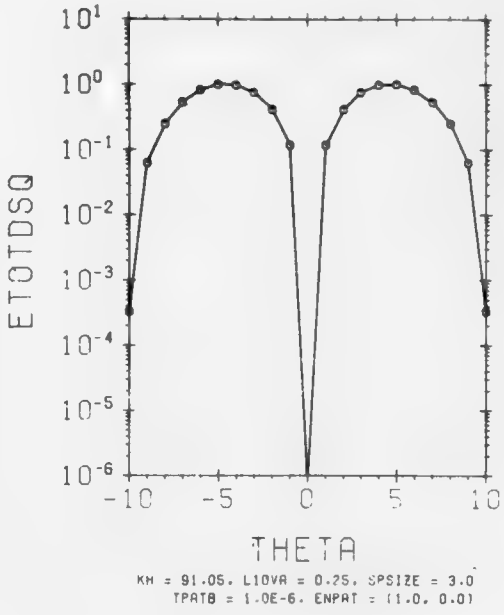

Figure 40. Difference Pattern of Rectangular Aperture (MIV), ENPAT = (1.0, 0.0), KH = 91.05

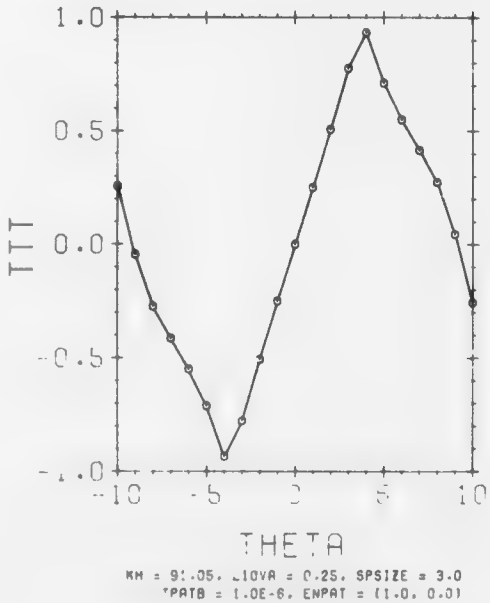

Figure 41. Tracking Signal (MIV), ENPAT = (1.0, 0.0), KH = 91.05

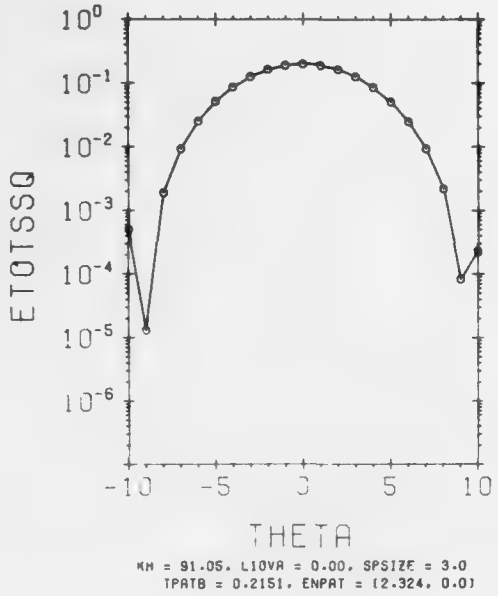

Figure 42. Sum Pattern of Rectangular Aperture (MIV), L1OVA = 0.00, KH = 91.05

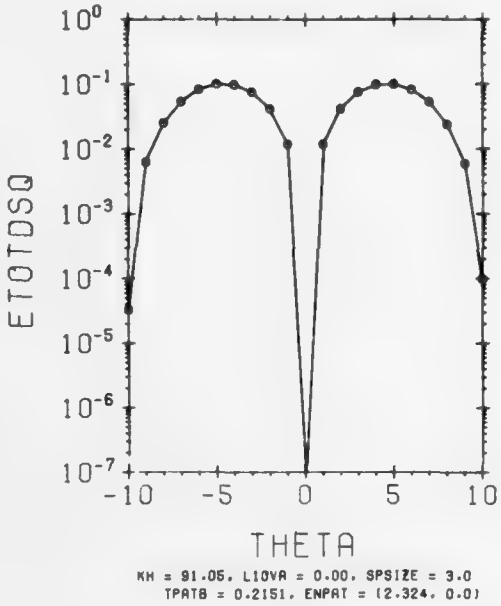

Figure 43. Difference Pattern of Rectangular Aperture (MIV), L1OVA = 0.00, KH = 91.05

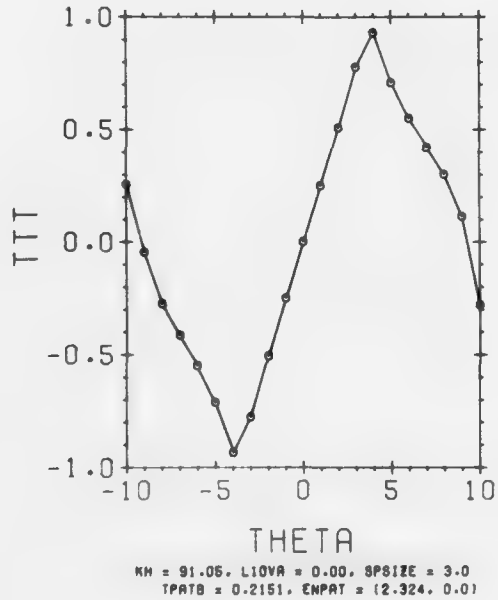

Figure 44. Tracking Signal (MIV), L1OVA = 0.00, KH = 91.05

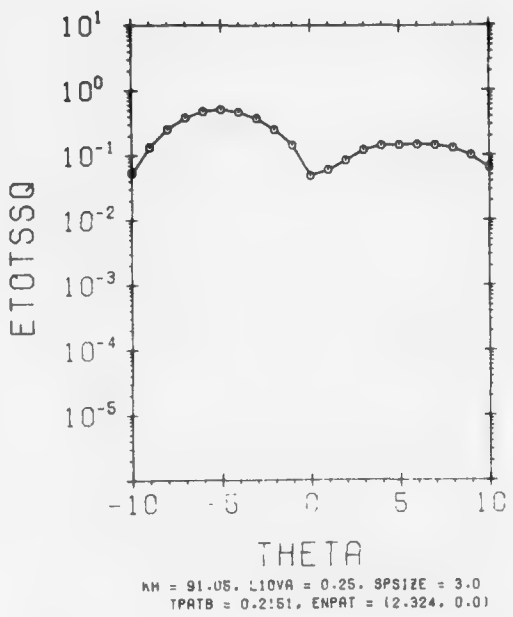

Figure 45. Sum Pattern of Rectangular Aperture (MIV), L1OVA = 0.25, KH = 91.05

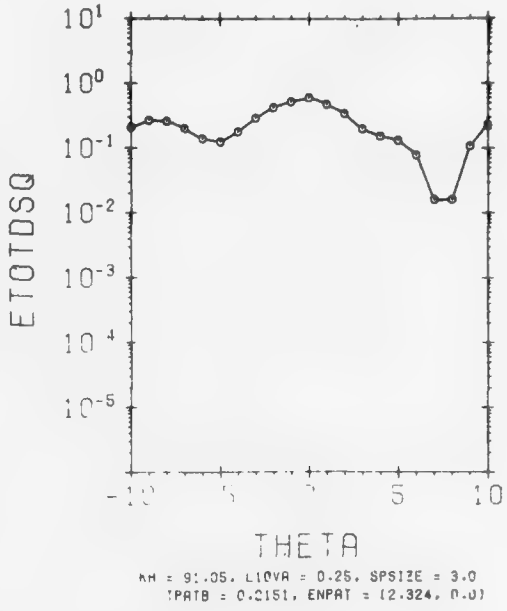

Figure 46. Difference Pattern of Rectangular Aperture (MIV), L1OVA = 0.25, KH = 91.05

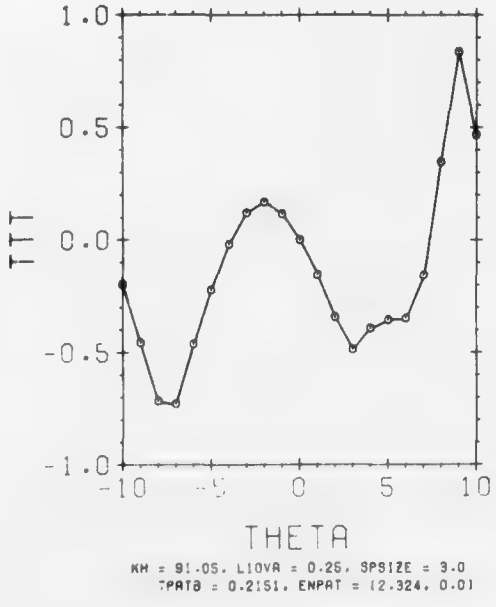

Figure 47. Tracking Signal (MIV), L1OVA = 0.25, KH = 91.05, ENPAT = (2.324, 0.0)

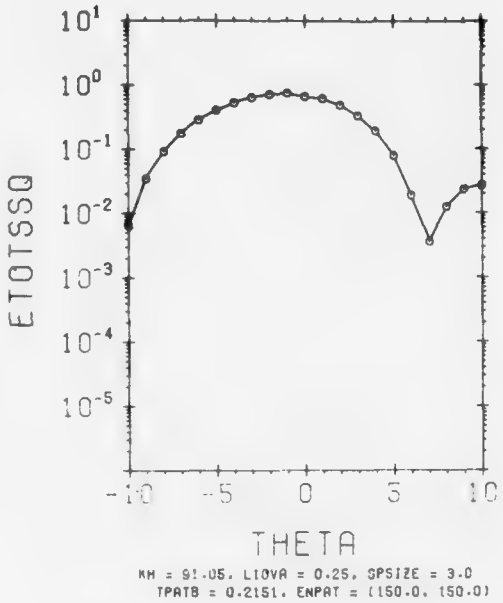

Figure 48. Sum Pattern of Rectangular Aperture (MIV), L1OVA = 0.25, KH = 91.05, ENPAT = (150.0, 150.0)

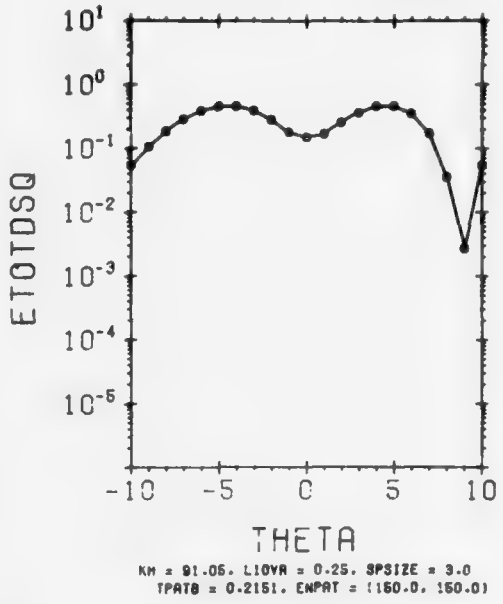

Figure 49. Difference Pattern of Rectangular Aperture (MIV), L1OVA = 0.25, KH = 91.05, ENPAT = (150.0, 150.0)

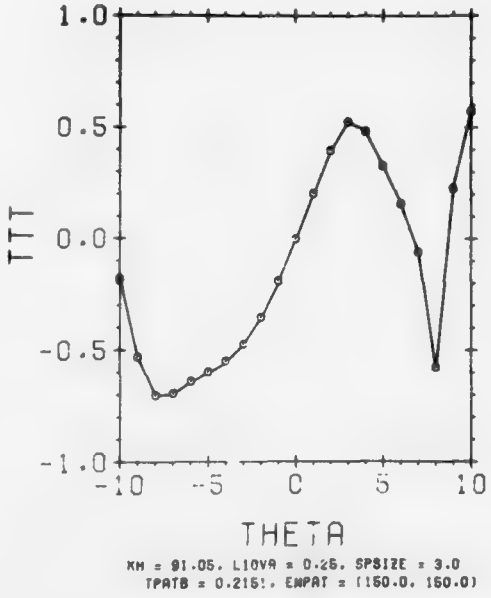

Figure 50. Tracking Signal (MIV), L1OVA = 0.25, KH = 91.05, ENPAT = (150.0, 150.0)

PHI = phase angle of transmission coefficient of patch ,

THETAO = θ_o ,

= half beamwidth of one beam in monopulse system .

TTT = tracking signal (defined in Eq. 1) ,

θ = polar angle with respect to vertical (z-axis) .

In Figure 51, the magnitude of the transmission coefficient of the patch TR = 1.0 and the phase angle of the patch's transmission coefficient PHI = 0.0°, so that there is effectively no patch. It should be noted that the tracking signal TTT equals +1 at $\theta = \theta_o$, which is the maximum value of TTT. Also, TTT = -1 at $\theta = -\theta_o$, TTT = 0.0 at $\theta = 0^o$, and TTT is anti-symmetric about $\theta = 0^o$. The slope $K_S = \frac{d(TTT)}{d\theta}$ is at its maximum when there is no patch (TR = 1, PHI = 0°).

In Figure 52 the parameters are the same as in Figure 51, except that TR = 0.5 instead of 1.0. A partially opaque patch with no phase shift upon transmission produces no distortion in TTT and no boresight shift, but there is a decrease in tracking sensitivity K_S. The parameters in Figure 53 are the same as in Figure 52, except that PHI = 45° instead of 0°. The partially opaque patch with a phase shift upon transmission reduces the tracking sensitivity K_S and, for this particular set of parameters, produces a small boresight shift (TTT = 0 does not occur exactly at $\theta = 0^o$).

In Figure 54, the parameters are the same as in Figure 52, but TR = 0.0 instead of 0.5. Comparing Figures 51, 52, and 54, it may be concluded that an asymmetrically located opaque patch with no phase shift upon transmission produces no boresight shift and the tracking sensitivity K_S decreases as the opacity increases.

In Figures 55 and 56, the parameters are the same as in Figure 51, except that in Figure 55, PHI = 45°, and in Figure 56, PHI = 90°, instead of PHI = 0°. Comparing Figures 51, 55, 56, it may be seen that increasing the phase shift of an asymmetrically located patch increases the boresight shift and decreases the tracking sensitivity.

In Figure 57, the parameters are the same as in Figure 51, except that TR = 0.5 and PHI = 180°, instead of TR = 1.0 and PHI = 0°. Also, in Figure 57, KLA = 0.0, so that the patch is symmetrically located in the aperture plane. It may be noted that although the patch is partially opaque and there is a 180° phase shift upon transmission, the symmetrically located patch produces virtually no change in the boresight axis and no decrease in K_S.

In Figure 58, the parameters are the same as in Figure 57, but the center of the patch is asymmetrically located over the aperture plane. Comparing Figure 58 with Figure 57 and Figure 51, it may be noted that a partially opaque

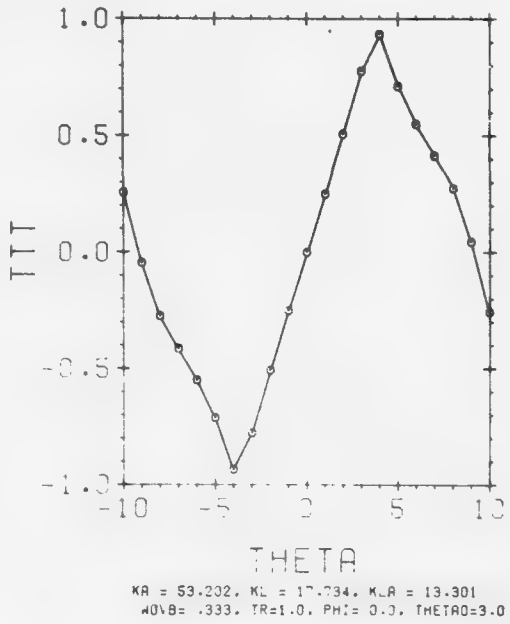

Figure 51. Tracking Signal (MV), TR = 1.0, PHI = 0.0° (no patch)

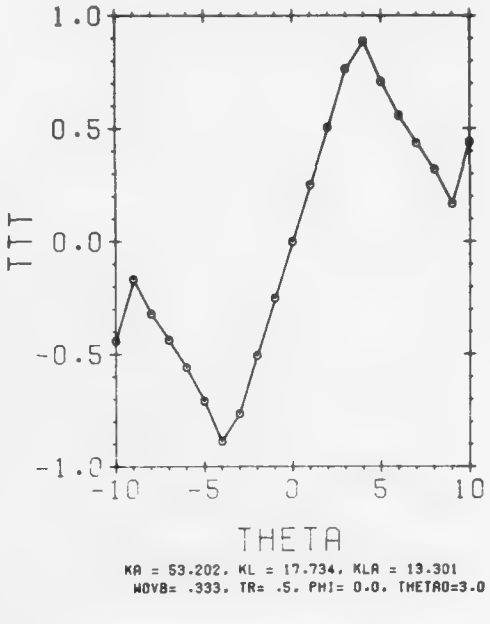

Figure 52. Tracking Signal (MV), TR = 0.5, PHI = 0.0° (no patch)

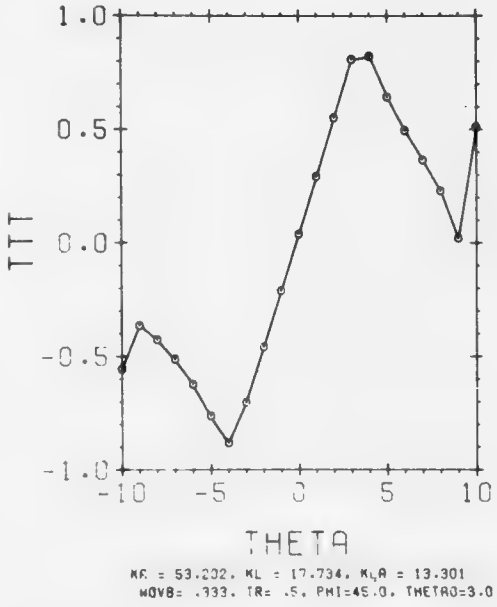

Figure 53. Tracking Signal (MV), PHI = 45°, TR = 0.5

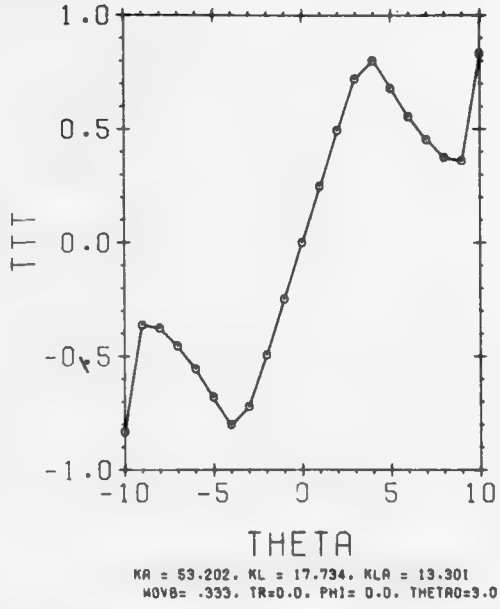

Figure 54. Tracking Signal (MV), TR = 0.0, PHI = 0.0° (no patch)

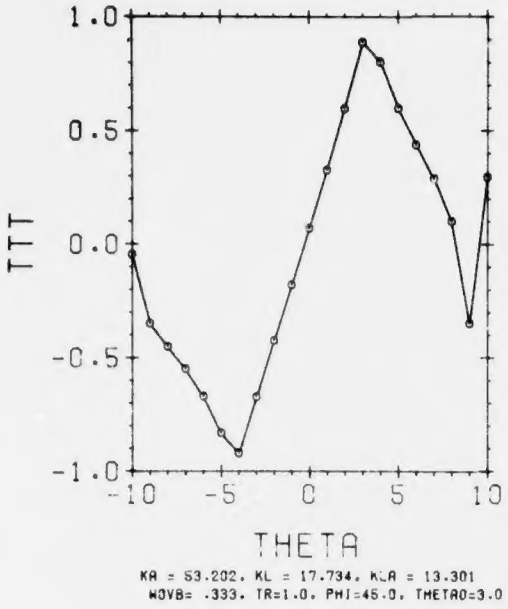

Figure 55. Tracking Signal (MV), TR = 1.0, PHI = 45.0°

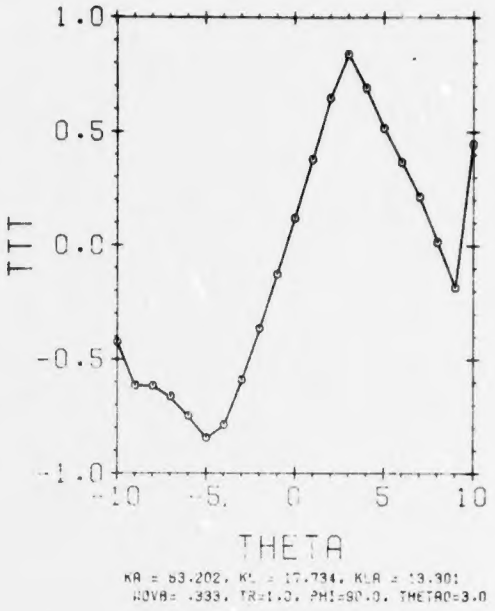

Figure 56. Tracking Signal (MV), TR = 1.0, PHI = 90.0°

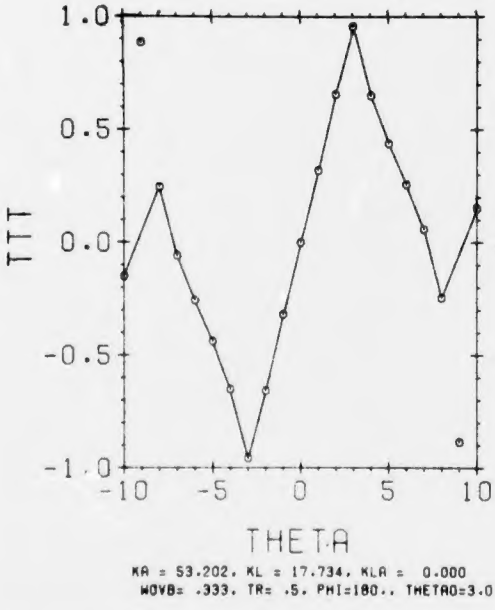

Figure 57. Tracking Signal (MV), TR = 0.5, PHI = 180°, KLA = 0.0

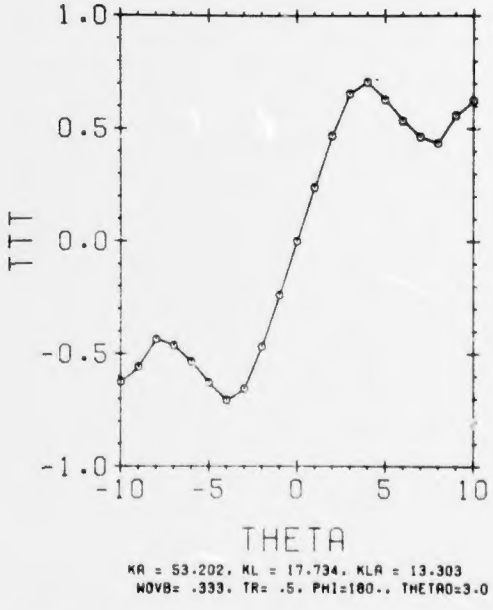

Figure 58. Tracking Signal (MV), TR = 0.5, PHI = 180°, KLA = 13.303

asymmetrically located patch with a 180^{o} phase shift upon transmission causes no boresight shift, but there is considerable loss of tracking sensitivity.

In order to calculate the uncertainty in boresight axis $\delta\theta$, caused by a noise source in the near field of an antenna according to Eq. (17), the following parameters must be defined:

KA = $(2\pi/\lambda)$A ,

A = aperture length ,

λ = free space wavelength ,

KB = $(2\pi/\lambda)$B ,

B = aperture width ,

KH = $(2\pi/\lambda)$H ,

H = height of patch center above aperture plane ,

KH = $(2\pi/\lambda)$H ,

L = length of patch area ,

KLA = $(2\pi/\lambda)$LA ,

LA = x-coordinate of rectangular patch area ,

LB = y-coordinate of rectangular patch area ,

$K_S = \frac{d(TTT)}{d\theta}$ = tracking sensitivity ,

BANDWID = bandwidth of receiver system ,

T_N = temperature of noise source in near field of monopulse antenna ,

TR = amplitude of transmission coefficient of patch ,

PHI = phase of transmission coefficient of patch ,

WOVB = W/B ,

W = width of rectangular patch ,

θ_B = beamwidth (half-power) of one beam of monopulse antenna ,

θ_o = inclination angle of one beam of monopulse antenna ,

G_{TR} = gain of ground based transmitting antenna ,

P_{TR} = power of transmitting antenna ,

$\overline{\sigma} = \sigma/\lambda^2$,

σ = cross section of target ,

$\overline{R}_1 = R_1/\lambda$,

R_1 = range from transmitting antenna to target ,

$\bar{R}_2$ = R_2/λ ,

R_2 = range from target to receiving antenna ,

G_{REC} = gain of receiver system ,

T^A_{SKY} = average sky temperature (given under Eq. 19) ,

T_{REC} = receiver system noise temperature .

Then, in calculating K_S and the gain of the monopulse receiving antenna with a partially blocked aperture, the model MV may be used. Equations (17) through (24) may be used to calculate ($\delta\theta$) the uncertainty in boresight axis caused by a noise source in the near field of a monopulse antenna. Values of $\delta\theta$ will be calculated for operational military systems in a classified note.

References

1. Papa, R.J. and Taylor, R.L. (1975) Effect of Radome Damage on Antenna Tracking Systems, AFCRL-TR-75-0541.
2. Wu, D.C.F. and Rudduck, R.C. (1974) IEEE Trans. on Antennas and Propagation, AP-22, No. 3:497.
3. Born, N. and Wolf, E. (1965) Principles of Optics, Pergamon Press.
4. Silver, S. (1949) Microwave Antenna Theory and Design, McGraw Hill.
5. Barton, D.K. (1964) Radar Systems Analysis, Prentice Hall.
6. McCormick, J.M. and Salvadori, M.G. (1964) Numerical Methods in Fortran, Prentice-Hall.